



ISIMIP3b bias adjustment fact sheet

Stefan Lange
December 1, 2021

Contents

1	Introduction	1
2	Observational dataset	1
3	Bias adjustment and statistical downscaling method	1
4	Differences between ISIMIP3BASD versions 1.0 and 2.5	3
5	Preprocessing of climate model output	5
6	Climate model selection	7
7	Results	8

If you use bias-adjusted ISIMIP3b climate input data then please cite (where applicable) Lange (2019) and Lange (2021) for the bias adjustment and statistical downscaling method ISIMIP3BASD, and Cucchi et al. (2020) and Lange et al. (2021) for the observational dataset W5E5.

Table 1: Specs of climate variables bias-adjusted and statistically downscaled for ISIMIP3b. Here, pr represents total precipitation (rainfall plus snowfall) while prsn represents snowfall, hence pr – prsn represents rainfall. Note that the upper limits of pr and prsn correspond to 600 mm day⁻¹ and 300 mm day⁻¹, respectively, while the lower and upper limits of tas, tasmx and tasmin correspond to –90 °C and +70 °C, respectively.

Variable	Short name	Unit	Limits
Near-Surface Relative Humidity	hurs	%	[1, 100]
Near-Surface Specific Humidity	huss	kg kg ⁻¹	[0.0000001, 0.1]
Precipitation	pr	kg m ⁻² s ⁻¹	[0, 0.0069444444]
Snowfall Flux	prsn	kg m ⁻² s ⁻¹	[0, 0.0034722222]
Surface Air Pressure	ps	Pa	[480, 110000]
Surface Downwelling Longwave Radiation	rlds	W m ⁻²	[40, 600]
Surface Downwelling Shortwave Radiation	rsds	W m ⁻²	[0, 500]
Near-Surface Wind Speed	sfcWind	m s ⁻¹	[0.1, 50]
Near-Surface Air Temperature	tas	K	[183.15, 343.15]
Daily Maximum Near-Surface Air Temperature	tasmx	K	[183.15, 343.15]
Daily Minimum Near-Surface Air Temperature	tasmin	K	[183.15, 343.15]

1 Introduction

This document describes the climate model selection, bias adjustment and statistical downscaling that was carried out to produce the climate input data for phase 3b of the Inter-Sectoral Impact Model Intercomparison Project (ISIMIP3b) based on output of phase 6 of the Coupled Model Intercomparison Project (CMIP6; Eyring et al., 2016). The document is structured as follows. It first describes the observational dataset (Sect. 2) and the methods (Sect. 3 and Sect. 4) used for bias adjustment and statistical downscaling. It then outlines how climate model output was preprocessed (Sect. 5) and how climate models were grouped into primary and secondary models (Sect. 6) and concludes with the discussion of selected results (Sect. 7).

2 Observational dataset

The observational reference dataset used for bias adjustment and statistical downscaling in ISIMIP3b is version 2.0 of WFDE5 over land merged with ERA5 over the ocean (W5E5; Cucchi et al., 2020; Lange et al., 2021). This dataset covers 1979–2019 at daily temporal resolution and the entire globe at 0.5° spatial resolution. Data sources of W5E5 are version 2.0 of WATCH Forcing Data methodology applied to ERA5 data (WFDE5; Weedon et al., 2014; Cucchi et al., 2020), ERA5 reanalysis data (Hersbach et al., 2020), and precipitation data from version 2.3 of the Global Precipitation Climatology Project (GPCP; Adler et al., 2003).

3 Bias adjustment and statistical downscaling method

The method used for bias adjustment and statistical downscaling in ISIMIP3b is ISIMIP3BASD v2.5 (Lange, 2021). Differences between this method version and ISIMIP3BASD v1.0 introduced in Lange (2019) are described in Sect. 4. Table 1 lists all variables that were adjusted and downscaled. From these variables, huss, prsn, tasmx and tasmin were adjusted and downscaled indirectly: huss was derived from adjusted and downscaled hurs, ps and tas, prsn was derived from adjusted and downscaled pr and prsnratio = prsn/pr, and tasmx and tasmin were derived from adjusted and downscaled tas, tasrange = tasmx – tasmin and tasskew = (tas – tasmin)/(tasmx – tasmin).

The training period used for both bias adjustment and statistical downscaling was 1979–2014. Like the training period, all application periods have a length of 36 years. Application periods used for piControl were 1601–1636, 1637–1672, 1673–1708, 1709–1744, 1745–1780, 1781–1816, 1817–1852, 1853–

```

python bias_adjustment.py
--step-size 1
--randomization-seed 0
-v relative_humidity,precipitation_flux,snowfall_flux,surface_air_pressure,
surface_downwelling_longwave_flux_in_air,surface_downwelling_shortwave_flux_in_air,
wind_speed,air_temperature,air_temperature,air_temperature
--lower-bound 0,0,0,,0,0,,0,0
--lower-threshold .01,.0000011574,.0001,,.0001,.01,,.01,.0001
--upper-bound 100,,1,,1,,,1
--upper-threshold 99.99,,.9999,,,9999,,,,.9999
--distribution ,gamma,,normal,normal,,weibull,normal,weibull,
-t bounded,mixed,bounded,additive,additive,bounded,mixed,additive,mixed,bounded
--unconditional-ccs-transfer 1,,,,,,
--trendless-bound-frequency 1,,,,,,
-d ,,1,1,,1,,
-w 0,0,0,0,0,15,0,0,0,0
--if-all-invalid-use ,,0,,,,,,
-o OBSinput/hurs_lowres_1979-2014.nc,OBSinput/pr_lowres_1979-2014.nc,
OBSinput/prsnratio_lowres_1979-2014.nc,OBSinput/ps_lowres_1979-2014.nc,
OBSinput/rlds_lowres_1979-2014.nc,OBSinput/rsds_lowres_1979-2014.nc,
OBSinput/sfcWind_lowres_1979-2014.nc,OBSinput/tas_lowres_1979-2014.nc,
OBSinput/tasrange_lowres_1979-2014.nc,OBSinput/tasskew_lowres_1979-2014.nc
-s GCMinput/hurs_lowres_1979-2014.nc,GCMinput/pr_lowres_1979-2014.nc,
GCMinput/prsnratio_lowres_1979-2014.nc,GCMinput/ps_lowres_1979-2014.nc,
GCMinput/rlds_lowres_1979-2014.nc,GCMinput/rsds_lowres_1979-2014.nc,
GCMinput/sfcWind_lowres_1979-2014.nc,GCMinput/tas_lowres_1979-2014.nc,
GCMinput/tasrange_lowres_1979-2014.nc,GCMinput/tasskew_lowres_1979-2014.nc
-f GCMinput/hurs_lowres_2065-2100.nc,GCMinput/pr_lowres_2065-2100.nc,
GCMinput/prsnratio_lowres_2065-2100.nc,GCMinput/ps_lowres_2065-2100.nc,
GCMinput/rlds_lowres_2065-2100.nc,GCMinput/rsds_lowres_2065-2100.nc,
GCMinput/sfcWind_lowres_2065-2100.nc,GCMinput/tas_lowres_2065-2100.nc,
GCMinput/tasrange_lowres_2065-2100.nc,GCMinput/tasskew_lowres_2065-2100.nc
-b GCMoutput/hurs_lowres_2065-2100.nc,GCMoutput/pr_lowres_2065-2100.nc,
GCMoutput/prsnratio_lowres_2065-2100.nc,GCMoutput/ps_lowres_2065-2100.nc,
GCMoutput/rlds_lowres_2065-2100.nc,GCMoutput/rsds_lowres_2065-2100.nc,
GCMoutput/sfcWind_lowres_2065-2100.nc,GCMoutput/tas_lowres_2065-2100.nc,
GCMoutput/tasrange_lowres_2065-2100.nc,GCMoutput/tasskew_lowres_2065-2100.nc

```

Figure 1: Python command used for bias adjustment of all variables listed in Table 1. Note that this is stylized for the application period 2065–2100.

```

python statistical_downscaling.py
--randomization-seed 0
-v relative_humidity
--lower-bound 0
--lower-threshold .01
--upper-bound 100
--upper-threshold 99.99
-o OBSinput/hurs_highres_1979-2014.nc
-s GCMoutput/hurs_lowres_2065-2100.nc
-f GCMoutput/hurs_highres_2065-2100.nc

```

Figure 2: Python command used for statistical downscaling of hurs. Note that this is stylized for the application period 2065–2100.

1888, 1889–1924, 1925–1960, 1961–1996, 1997–2032, 2033–2068 (keeping 2033–2066), and 2065–2100 (keeping 2067–2100). Application periods used for historical were 1850–1885, 1886–1921, 1922–1957, 1958–1993, and 1994–2029 (combining historical and ssp585, keeping 1994–2014). Application periods used for ssp126, ssp370 and ssp585 were 2015–2050 (keeping 2015–2043), 2040–2075 (keeping 2044–2072), and 2065–2100 (keeping 2073–2100). The training period was not used as an application period to avoid overfitting artifacts.

Before bias adjustment and statistical downscaling, original CMIP6 output was interpolated in time and space. In order to harmonize calendars to the proleptic Gregorian calendar, missing days were inserted using linear interpolation in time. The spatial interpolation was necessary to make the ISIMIP3BASD statistical downscaling method applicable. It was done using first-order conservative remapping (Jones, 1999) to a regular latitude–longitude grid with 0.5° , 1.0° or 2.0° resolution, depending on which was closest to the resolution of the original output (Table 2 shows which resolution was used for which climate model).

Data interpolated to 0.5° were bias-adjusted using W5E5 data at 0.5° spatial resolution. Data interpolated to 1.0° were first bias-adjusted using W5E5 data aggregated to 1.0° and then downscaled to 0.5° using W5E5 data at 0.5° spatial resolution. Data interpolated to 2.0° were first bias-adjusted using W5E5 data aggregated to 2.0° and then downscaled in two steps using W5E5 data at 1.0° and 0.5° spatial resolution. See Figure 1 and Figure 2 for the python commands used for bias adjustment and statistical downscaling, respectively.

After bias adjustment and statistical downscaling, the limits listed in Table 1 were enforced for all variables, i.e., values greater/less than the upper/lower limit were set to the upper/lower limit.

4 Differences between ISIMIP3BASD versions 1.0 and 2.5

The development of ISIMIP3BASD from version 1.0 described in Lange (2019) to version 2.5 has considerably improved the method and its utility. For a complete list of differences between the two versions, see the CHANGELOG included in the archive of code version 2.5 (Lange, 2021). The most important developments are described in the following.

Both technical and methodical developments led to v2.0. First, all major performance and I/O bottlenecks were identified and removed from the code. This reduced the typical run time from months to days. Secondly, harnessing the embarrassingly parallel nature of the bias adjustment and statistical downscaling problem, memory usage was greatly reduced. Provided that all input NetCDF files are suitably chunked, v2.0 loads data lazily, only allocating memory for data from one grid cell at a time as the code loops over them for bias adjustment or statistical downscaling.

Thirdly, as already announced in Lange (2019), an option for the multivariate bias adjustment of several climate variables was added in v2.0, based on the MBCn algorithm by Cannon (2017). However, this option was not used in ISIMIP3b because it was found to produce overfitting artifacts (Figure 3) and impair spatial coherence (Figure 4) when applied to bias-adjust the joint distribution of 10 climate variables. The likely reason for the first issue is that the observational reference data only cover 36 years. This means that for every calendar month there are only about 1000 data points available to determine the 10-dimensional joint distribution function of the daily climate data. Since that is only about one data point per orthant in 10 dimensions, which is too small a sample for the task, hence the overfitting (Figure 3). The spatial coherence is impaired because the MBCn algorithm adjusts the multivariate rank distribution by suitably shuffling all univariate rank time series. When this is done independently in every grid cell, different shufflings are applied to the same climate variable in different grid cells. The result is spatial noise (Figure 4).

In v2.1, the method used for the detrending of ps, rlds and tas prior to quantile mapping was made conditional on the estimated trend being significantly (at the 5% level) different from zero. In v2.2, the randomization of values beyond threshold was changed because using a power-law distribution for the randomization sometimes led to numerical instabilities. The new randomization replaces all values beyond threshold by random numbers which are uniformly distributed between threshold and bound and sorted like the original values. An option to use non-parametric quantile mapping for bias adjustment was introduced in v2.3. It improved the bias adjustment of all variables which have both

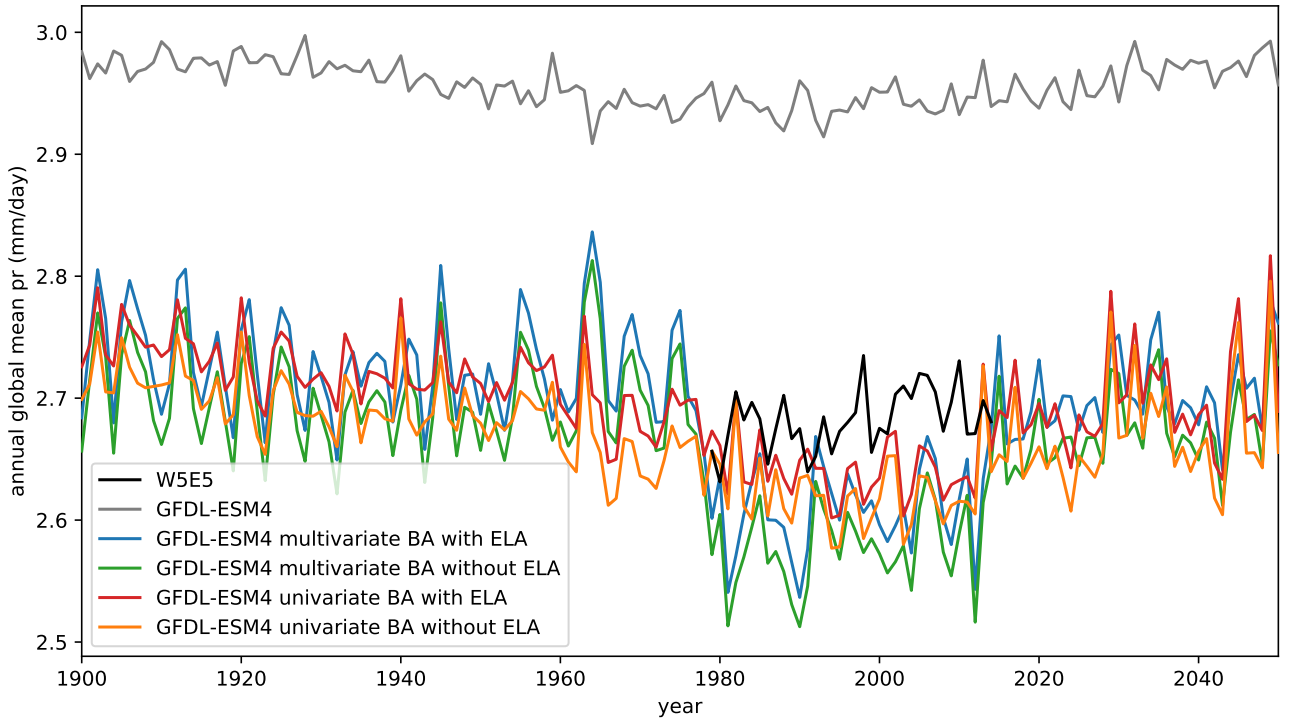


Figure 3: Annual global mean precipitation for GFDL-ESM4 historical and SSP5-8.5, with raw data in gray, bias-adjusted data in colors, and observational reference data in black. Colors distinguish results of multivariate and univariate bias adjustment (BA) with and without event likelihood adjustment (ELA). Discontinuities at the edges of the reference period (1979–2014) indicate overfitting.

a lower bound and an upper bound (hurs, prsnratio, rsds, tasskew). The previously used parametric quantile mapping suffered from occasionally unstable beta distribution fits.

The method used to generate pseudo future observations of bounded variables (Eqs. (8) and (9) of Lange (2019) was changed in v2.3 to stabilize results in some edge cases. The most important of those cases is the following. Let the historically observed relative dry-day frequency be 0.0 and let the simulated frequency be 0.8 for the historical period and 0.9 for some future period. Then, according to Eq. (9) of Lange (2019), the future pseudo-observed frequency would be equal to $1 - (1 - 0.0)(1 - 0.9)/(1 - 0.8) = 0.5$, which is probably unrealistic, given the large bias of the historically simulated value. The revised version of Eq. (9) of Lange (2019) introduced in v2.3 reads

$$P_{\text{fut}}^{\text{obs}} = \begin{cases} P_{\text{fut}}^{\text{sim}} & \text{if } P_{\text{hist}}^{\text{sim}} = P_{\text{hist}}^{\text{obs}}, \\ 0 + (P_{\text{hist}}^{\text{obs}} - 0) (P_{\text{fut}}^{\text{sim}} - 0) / (P_{\text{hist}}^{\text{sim}} - 0) & \text{if } P_{\text{fut}}^{\text{sim}} \leq P_{\text{hist}}^{\text{sim}} > P_{\text{hist}}^{\text{obs}}, \\ 1 - (1 - P_{\text{hist}}^{\text{obs}}) (1 - P_{\text{fut}}^{\text{sim}}) / (1 - P_{\text{hist}}^{\text{sim}}) & \text{if } P_{\text{fut}}^{\text{sim}} \geq P_{\text{hist}}^{\text{sim}} < P_{\text{hist}}^{\text{obs}}, \\ P_{\text{hist}}^{\text{obs}} + P_{\text{fut}}^{\text{sim}} - P_{\text{hist}}^{\text{sim}} & \text{otherwise.} \end{cases} \quad (1)$$

In this revised relation, the otherwise case applies if $P_{\text{fut}}^{\text{sim}} < P_{\text{hist}}^{\text{sim}} < P_{\text{hist}}^{\text{obs}}$ or $P_{\text{fut}}^{\text{sim}} > P_{\text{hist}}^{\text{sim}} > P_{\text{hist}}^{\text{obs}}$. Hence it applies to the aforementioned edge case, where it produces a less extreme future pseudo-observed relative frequency of $0.0 + 0.9 - 0.8 = 0.1$. Equation (8) of Lange (2019) was revised similarly, given the similar structure of the two equations.

The method used to generate pseudo future observations (step 5 of the bias adjustment algorithm of Lange 2019) was further refined in v2.4 for all variables with at least one bound. Before v2.4, the pseudo future observations were generated by transferring simulated trends in all distribution quantiles to the observational reference data. However, that included trends in, e.g., precipitation quantiles below the wet-day threshold. In some cases, the trend transfer turned many dry days into wet days, with a profound impact on the shape of the pseudo future wet-day precipitation distribution. As a result, simulated trends in wet-day precipitation intensity were not well preserved. In v2.4, trend transfers were restricted to values within threshold. This particularly improved the preservation of trends in wet-day precipitation intensity.

GFDL-ESM4 historical bias-adjusted rsds for 01 January 2011

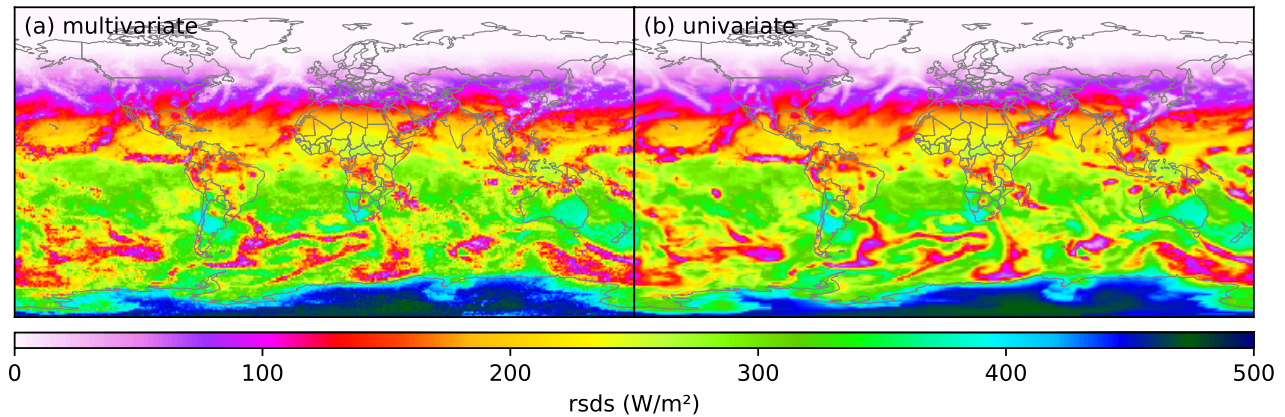


Figure 4: GFDL-ESM4 historical surface downwelling shortwave radiation for 01 January 2011 bias-adjusted (a) multivariately with 9 other climate variables and (b) univariately.

The bias adjustment method for hurs was changed in v2.5 because previous method versions produced unrealistic distributions under climate change if there are too many supersaturations ($\text{hurs} \geq 100\%$) in the simulated data. This occurs in several of the CMIP6 GCMs selected for ISIMIP3b, particularly in high-latitude winter. An example is given in Figure 5: while no supersaturations occur in the observational reference data, the GCM simulates many supersaturations in the historical reference period and even more so in a future period under SSP5-8.5. Previous method versions preserved this projected trend and hence produced future bias-adjusted hurs data with many supersaturations. In v2.5, this trend is no longer preserved. Instead, the supersaturation probability is fixed at the observed level, which is zero or very close to zero in all seasons and grid cells for W5E5. Furthermore, v2.5 generates pseudo-future hurs observations by applying Eq. (1) to all hurs values after capping them at 100%. Those two changes were motivated by findings from Ruosteenoja et al. (2017, 2018). They analysed hurs data from CMIP5 and showed that (i) supersaturations in those data are mostly spurious, resulting from, e.g., inconsistencies in the interpolation of temperature and specific humidity to the near-surface level, and (ii) climatological mean value trends of hurs become more consistent with trends in relative humidity from the lowest model level if hurs is capped at 100% before trends are calculated.

Last but not least, an option to use running windows instead of fixed monthly windows for seasonal bias adjustment was added in v2.5. The running-window mode was introduced because the month-by-month bias adjustment described in Lange (2019) was found to produce discontinuities in statistics such multi-year daily mean values at each turn of the month (Figure 6). For ISIMIP3b, the running window used has a width of 31 days. This window is moved over the annual cycle in steps of 1 day. Results for the central day of each window constitute the overall result. This application pattern solves the discontinuity issue (Figure 6), as suggested by Themeßl et al. (2012); Thrasher et al. (2012); Gennaretti et al. (2015); Grenier (2018).

Note also that the event likelihood adjustments described in Lange (2019) were not applied for any variable to prevent overfitting artifacts (Figure 3). In addition, the diurnal temperature range was ultimately bias-adjusted using a Weibull distribution, not a Rice distribution as described in Lange (2019) because the Weibull distribution turned out to fit the data better in most cases, in particular in the upper tail.

5 Preprocessing of climate model output

Next to the temporal and spatial interpolation already mentioned in Sect. 3, raw CMIP6 output was harmonized in terms of variable coverage and piControl periods.

If for a given model ps data were not available for at least one experiment but psl (Sea Level Pressure) data were available for all experiments then a proxy of ps was used for all experiments. This

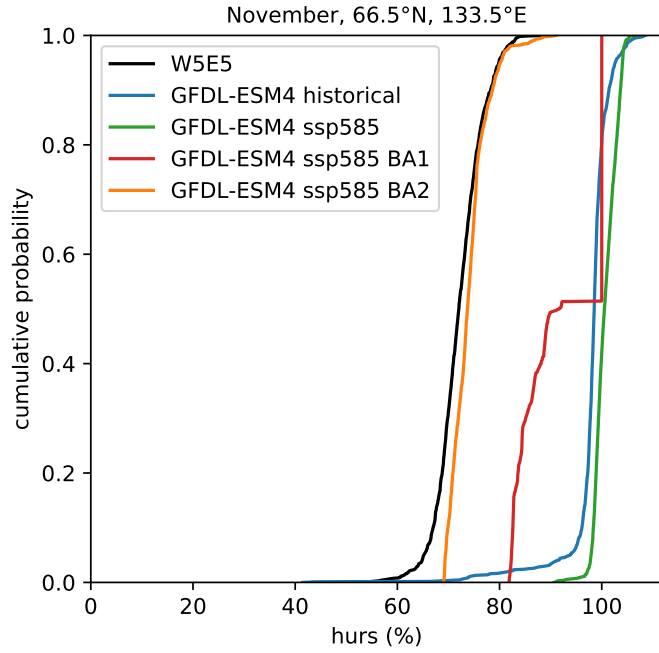


Figure 5: Empirical cumulative distribution functions of near-surface relative humidity in high-latitude winter (November, 66.5°N, 133.5°E) for GFDL-ESM4 historical (1979–2014) and SSP5-8.5 (2065–2100), with historical simulated data in blue, future simulated data in green, future bias-adjusted data in red and orange, and observational reference data in black. The simulated climate change signal is well preserved with ISIMIP3BASD v2.5 using a fixed supersaturation ($\text{hurs} \geq 100\%$) probability and Eq. (1) applied to all hurs values after capping them at 100% to generate pseudo-future observations (orange). In contrast, the simulated climate change signal is not well preserved if the supersaturation probability is allowed to change and Eqs. (8) and (9) of Lange (2019) are used to generate pseudo-future hurs observations (red).

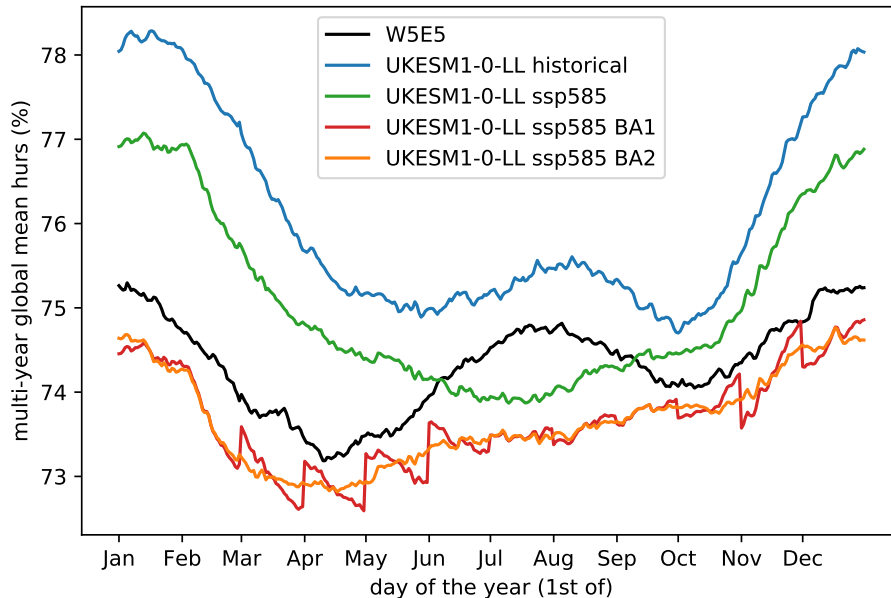


Figure 6: Global multi-year daily mean near-surface relative humidity for UKESM1-0-LL historical (1979–2014) and SSP5-8.5 (2065–2100), with historical simulated data in blue, future simulated data in green, future bias-adjusted data in red and orange, and observational reference data in black. A smooth annual cycle is produced if ISIMIP3BASD v2.5 is applied in running-window mode in steps of one day (orange). In contrast, a month-by-month application generates discontinuities at each turn of the month (red).

Table 2: Specs of CMIP6 climate models included in ISIMIP3b. Primary models are mandatory to use by the ISIMIP impact modelling teams. Secondary models are optional. The third column shows the spatial resolution that the original data was interpolated to prior to bias adjustment and statistical downscaling. The fourth column shows which ensemble member was used. The fifth column shows which year labels were attached to the original piControl data used for ISIMIP3b. The last two columns indicate whether ps and sfcWind data were directly available or needed to be approximated from other available output using Eq. (2) for ps and Eq. (3) for sfcWind. Note that the model order in this table is alphabetical, i.e., no ranking within the groups is implied.

Model	Group	Resolution	Member	piControl	ps	sfcWind
GFDL-ESM4	primary	1.0°	r1i1p1f1	0001–0500	available	available
IPSL-CM6A-LR	primary	2.0°	r1i1p1f1	1870–2369	available	available
MPI-ESM1-2-HR	primary	1.0°	r1i1p1f1	1850–2349	available	available
MRI-ESM2-0	primary	1.0°	r1i1p1f1	1850–2349	proxy	available
UKESM1-0-LL	primary	2.0°	r1i1p1f2	1960–2459	available	available
CanESM5	secondary	2.0°	r1i1p1f1	5201–5700	proxy	available
CNRM-CM6-1	secondary	1.0°	r1i1p1f2	1850–2349	proxy	proxy
CNRM-ESM2-1	secondary	1.0°	r1i1p1f2	1850–2140	proxy	proxy
EC-Earth3	secondary	0.5°	r1i1p1f1	2259–2758	proxy	available
MIROC6	secondary	1.0°	r1i1p1f1	3200–3699	proxy	proxy

proxy was computed according to

$$ps = psl \exp\left(-\frac{g \text{ orog}}{R_{tas}}\right), \quad (2)$$

where orog is the climate model orography, g is gravity and R is the specific gas constant of dry air. Similarly, if sfcWind data were not available for at least one experiment but uas and vas (Eastward and Northward Near-Surface Wind) data were available for all experiments then a proxy of sfcWind was used for all experiments. This proxy was computed according to

$$\text{sfcWind} = \sqrt{\text{uas}^2 + \text{vas}^2}. \quad (3)$$

Whether ps and sfcWind data were directly available or needed to be approximated for a given model is shown in Table 2.

Since piControl starts in different years for different models, piControl data were shifted in time to a harmonized ISIMIP3b piControl period of 1601–2100. The original piControl periods used are shown in Table 2. If fewer than 500 years worth of piControl data were available for a given model then the available data were recycled until 500 years were reached. This was only necessary for CNRM-ESM2-1, which provided 291 years worth of piControl data.

6 Climate model selection

CMIP6 experiments used in ISIMIP3b are piControl, historical, ssp126, ssp370 and ssp585. In order to be included in ISIMIP3b, a climate model had to provide daily data for all variables listed in Table 1 except huss (not needed), ps (if psl was available) and sfcWind (if uas and vas were available) for at least 250 years in piControl and for all years in historical (1850–2014), ssp126, ssp370 and ssp585 (2015–2100).

The models fulfilling these data availability criteria were divided into primary and secondary models. The list of primary models was fixed at the beginning of ISIMIP3b. These models are mandatory to use by the ISIMIP impact modelling teams. The list of secondary models is open and can be extended as more CMIP6 output becomes available during ISIMIP3b. These models are optional to use. The selection of primary models was done taking into account process representation, structural independence, climate sensitivity, performance in the historical period as well as the special input data needs of the fisheries and marine ecosystems sector (FishMIP).

Performance in the historical period was assessed using the portrait plot depicted in Figure 7. According to this plot, the better-performing CMIP6 models are *AWI-CM-1-1-MR*, *CESM2*, *CESM2-WACCM*, *GFDL-CM4*, *GFDL-ESM4*, *HadGEM3-GC31-LL*, *MPI-ESM1-2-HR*, *MPI-ESM1-2-LR*, *MRI-ESM2-0*, *SAM0-UNICON* and *UKESM1-0-LL*. In the previous list, models in italics are those which did not provide all data needed in ISIMIP3b. This leaves *GFDL-ESM4*, *MPI-ESM1-2-HR*, *MRI-ESM2-0* and *UKESM1-0-LL* as potential primary models. Three of these also provide data for the essential ocean variables for FishMIP. Another model providing data for these variables is *IPSL-CM6A-LR*. It was decided that these five models are the primary models of ISIMIP3b.

The five primary models are a good choice because they are structurally independent in terms of their ocean and atmosphere model components and because, according to an informal survey among experts from the CRESCENDO project, their process representation is fair (*IPSL-CM6A-LR*, *MPI-ESM1-2-HR*) to good (*GFDL-ESM4*, *MRI-ESM2-0*, *UKESM1-0-LL*). In terms of climate sensitivity (Figure 8), the five primary models are good representatives of the whole CMIP6 ensemble as they include three models with low climate sensitivity (*GFDL-ESM4*, *MPI-ESM1-2-HR*, *MRI-ESM2-0*) and two models with high climate sensitivity (*IPSL-CM6A-LR*, *UKESM1-0-LL*). Also, three models (*GFDL-ESM4*, *IPSL-CM6A-LR*, *UKESM1-0-LL*) are successors of models used in ISIMP2b and in the ISIMIP Fast Track, which is beneficial in terms of tracibility.

7 Results

Bias adjustment and statistical downscaling results are shown here using only a few selected control plots. Figure 8 shows projected changes in annual global mean precipitation and temperature before and after bias adjustment and statistical downscaling. The results demonstrate the ISIMIP3BASD preserves the simulated warming signal. Since ISIMIP3BASD preserves precipitation trends multiplicatively in most cases, the bias adjustment has altered absolute precipitation changes. The plot also shows that the spectrum of simulated global mean temperature changes is well represented by the primary models.

Time series of global annual mean values before and after bias adjustment and statistical downscaling are shown in Figures 9, 12, 15, 18, 21, 24, 27, 30, 33 and 36 for all variables listed in Table 1 and all models listed in Table 2. They demonstrate that mean values were well adjusted in most cases. Biases only remain for prsn. In addition, for CanESM5, there are discontinuities visible in the prsn time series under ssp585.

Similar plots for global annual minimum values are shown in Figures 10, 13, 16, 19, 22, 25, 28, 31, 34 and 37. The adjustment of minimum values worked well for ps, pr, prsn, rsds, tas, tasmax and tasmin. It did not work too well for hurs, huss, sfcWind and rlds as for these variables rather often the limits given in Table 1 had to be enforced in post-processing. Reasons for this include the general imperfection of parametric quantile mapping, the imperfect generation of pseudo future observations (Lange, 2019) and the alteration of bias-adjusted values by statistical downscaling.

Time series of global annual maximum values are shown in Figures 11, 14, 17, 20, 23, 26, 29, 32, 35 and 38. The adjustment of maximum values worked well for huss, ps, rsds, tas and tasmin. It worked rather well for rlds. It did not work too well for hurs, pr, prsn, sfcWind and tasmax as for these variables rather often the limits given in Table 1 had to be enforced in post-processing, for the same reasons as in the case of the global annual minimum values.

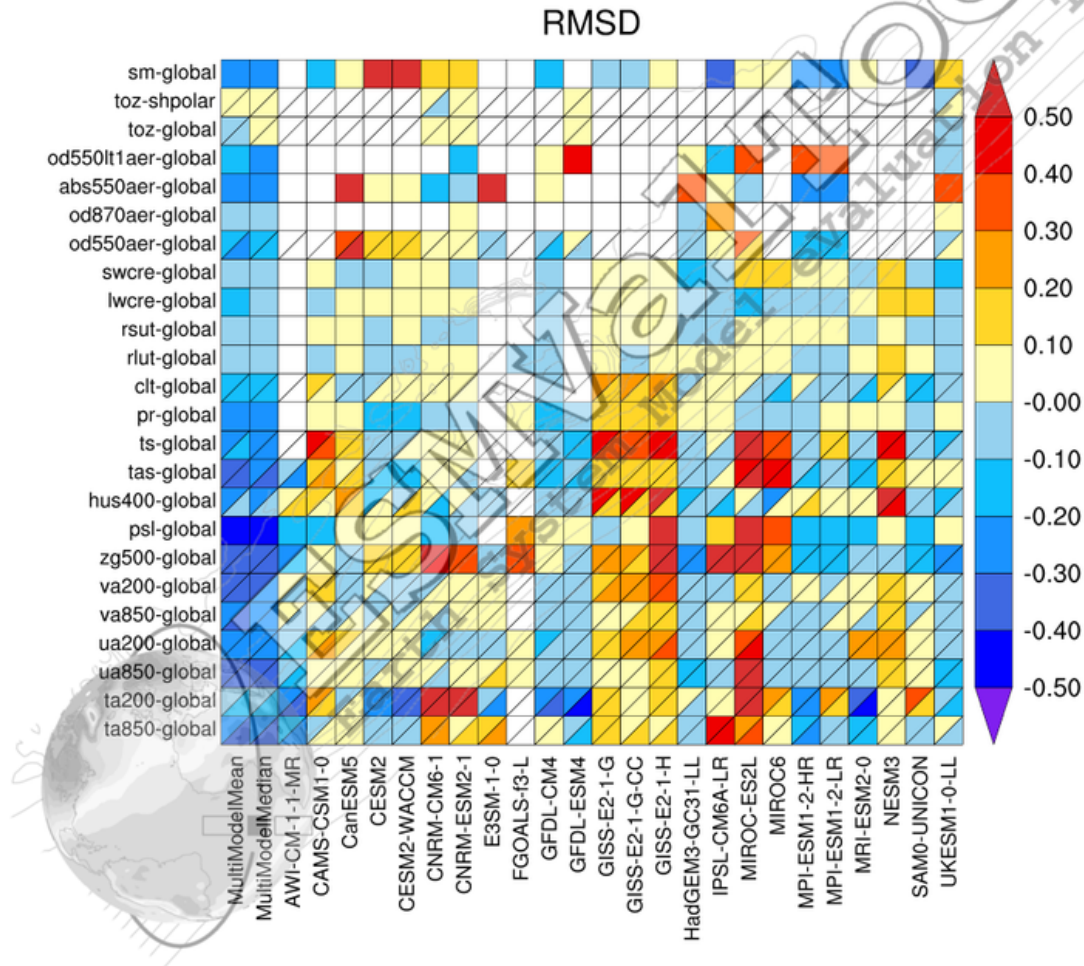


Figure 7: Portrait plot (Gleckler et al., 2008) of CMIP6 climate model performance for different models (columns) and variables (rows). The metric used as the basis of the plot is the root mean square difference (RMSD) between historical simulation and observation. Where cells are divided into triangles, two observational reference datasets were used. Monthly mean climatologies were used to compute the RMSD. These were then aggregated over calendar months and grid cells. Aggregation over all grid cells are indicated by the suffix -global, those over southern hemisphere polar grid cells only (60–90 °S) by -shpolar. RMSDs are expressed relative to the median model RMSD. White triangles or squares are due to missing data. Variables included are (from top to bottom) sm (Soil Moisture), toz (Total Ozone Column), od550lt1aer (Ambient Fine Aerosol Optical Depth at 550 nm), abs550aer (Ambient Aerosol Absorption Optical Thickness at 550 nm), od870aer (Ambient Aerosol Optical Depth at 870 nm), od550aer (Ambient Aerosol Optical Thickness at 550 nm), swcre (Shortwave Cloud Radiative Effect), lwcre (Longwave Cloud Radiative Effect), rsut (Top-of-Atmosphere Outgoing Shortwave Radiation), rlut (Top-of-Atmosphere Outgoing Longwave Radiation), clt (Total Cloud Cover Percentage), pr (Precipitation), tas (Near-Surface Air Temperature), hus400 (Specific Humidity at 400 hPa), psl (Sea Level Pressure), zg500 (Geopotential Height at 500 hPa), va200 (Northward Wind at 200 hPa), va850 (Northward Wind at 850 hPa), ua200 (Eastward Wind at 200 hPa), ua850 (Eastward Wind at 850 hPa), ta200 (Air Temperature at 200 hPa), ta850 (Air Temperature at 850 hPa). This plot was created on January 24, 2020 with ESMValTool v2.0.0b2.

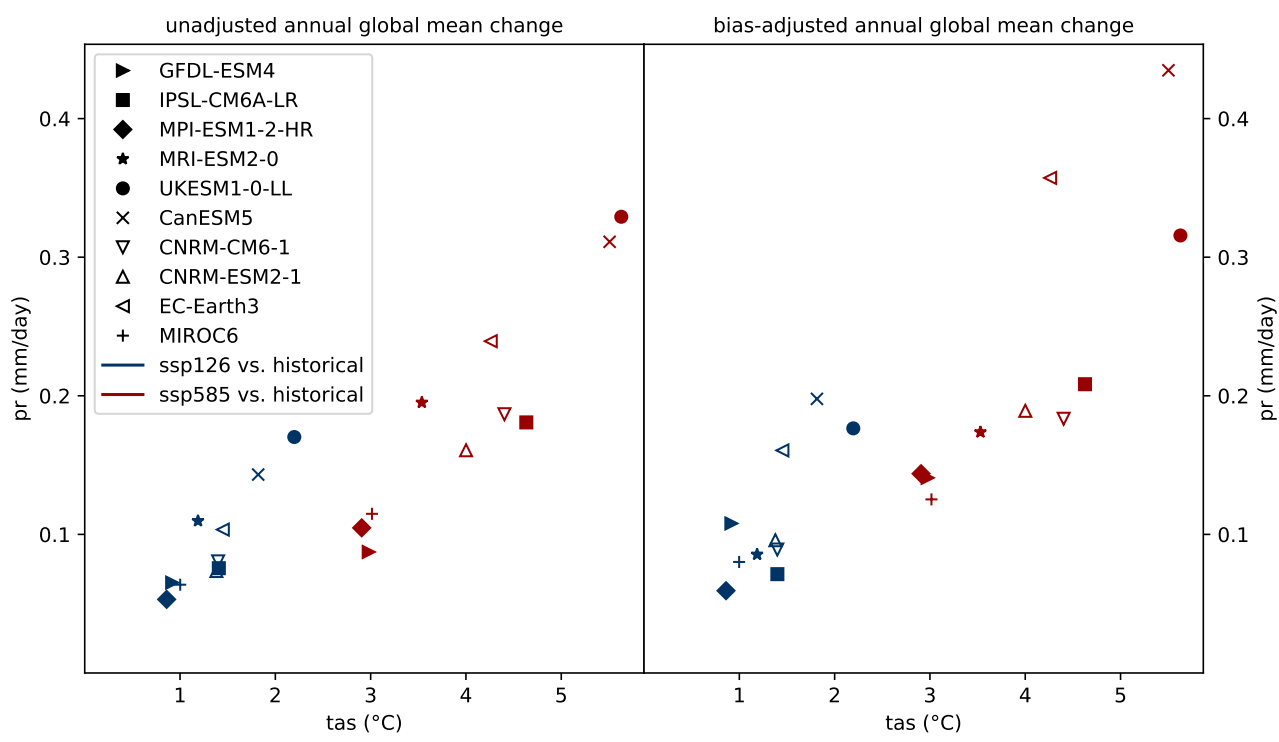


Figure 8: Projected change in annual global mean precipitation versus temperature computed based on unadjusted (left) and bias-adjusted (right) CMIP6 data. Results for different climate models are indicated with different symbols. For the primary models, these symbols are filled. Results for different future greenhouse gas emissions scenarios are indicated with different colors. Changes are computed as the difference between 30-year mean values (2071–2100 versus 1985–2014).

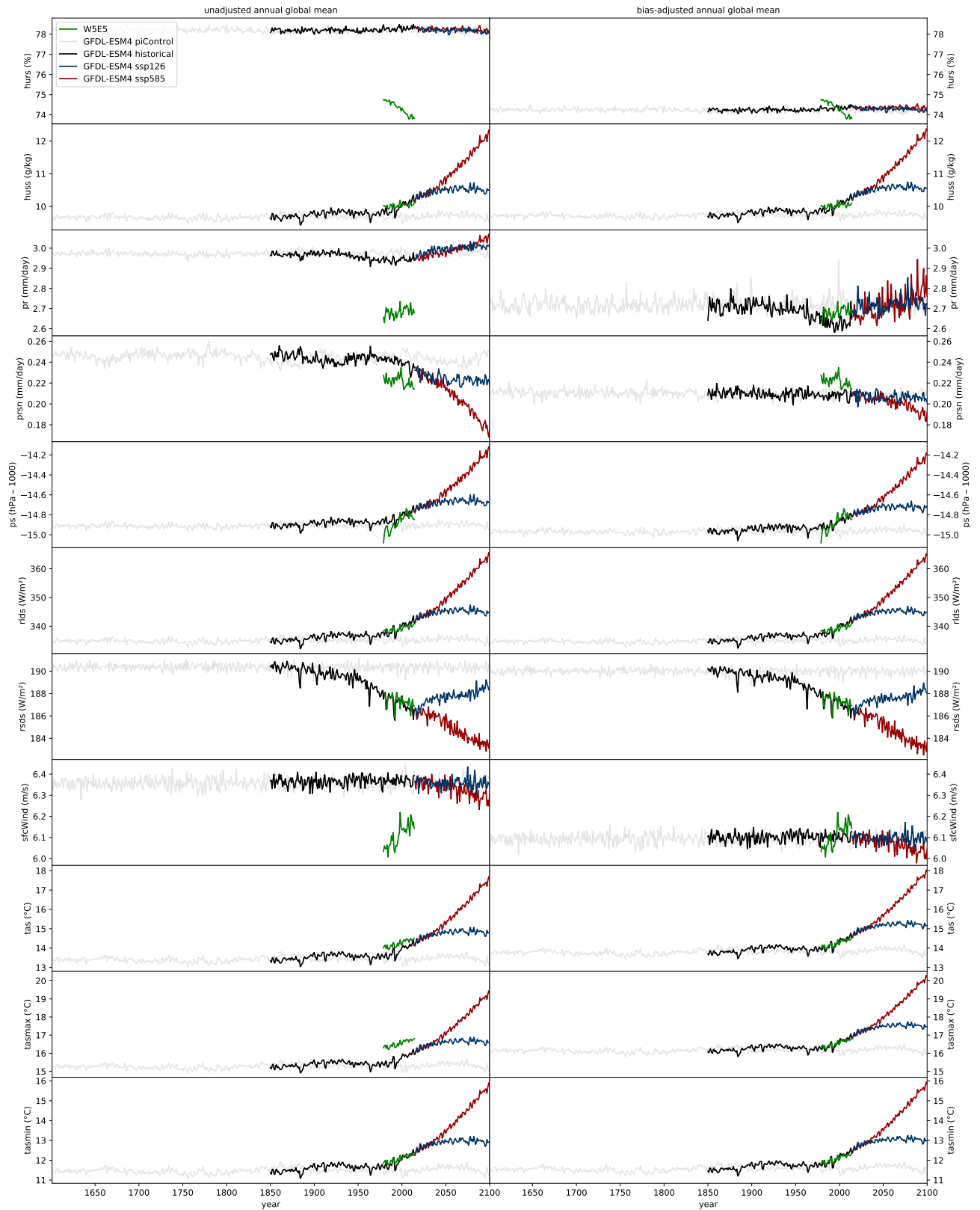


Figure 9: Unadjusted (left) and bias-adjusted (right) time series of annual global mean hurs, huss, pr, prsn, ps, rlds, rsds, sfcWind, tas, tasmax and tasmin (from top to bottom) for W5E5 (green) and GFDL-ESM4 (other colors for different CMIP6 experiments).

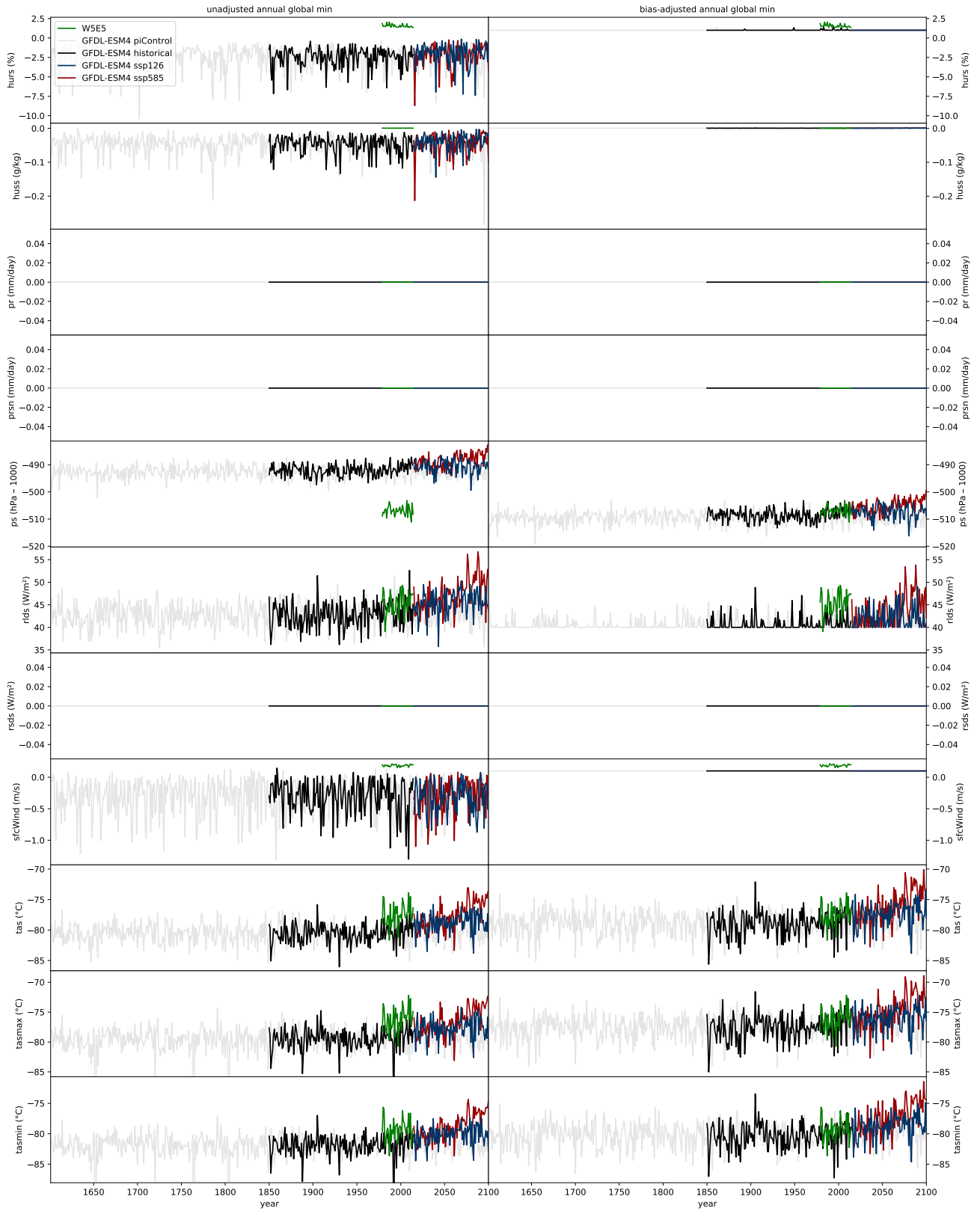


Figure 10: Same as Figure 9 but for annual global minimum values.

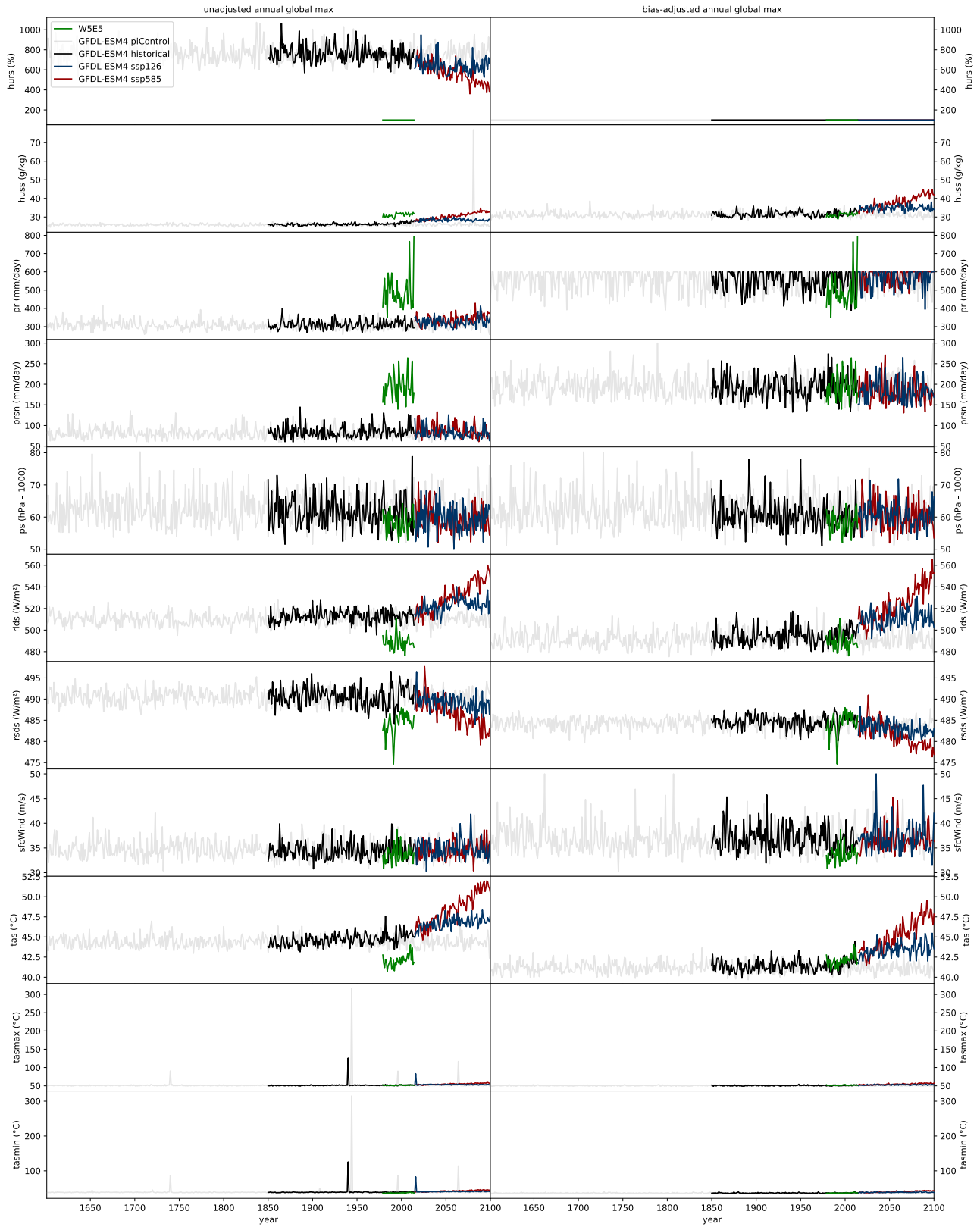


Figure 11: Same as Figure 9 but for annual global maximum values.

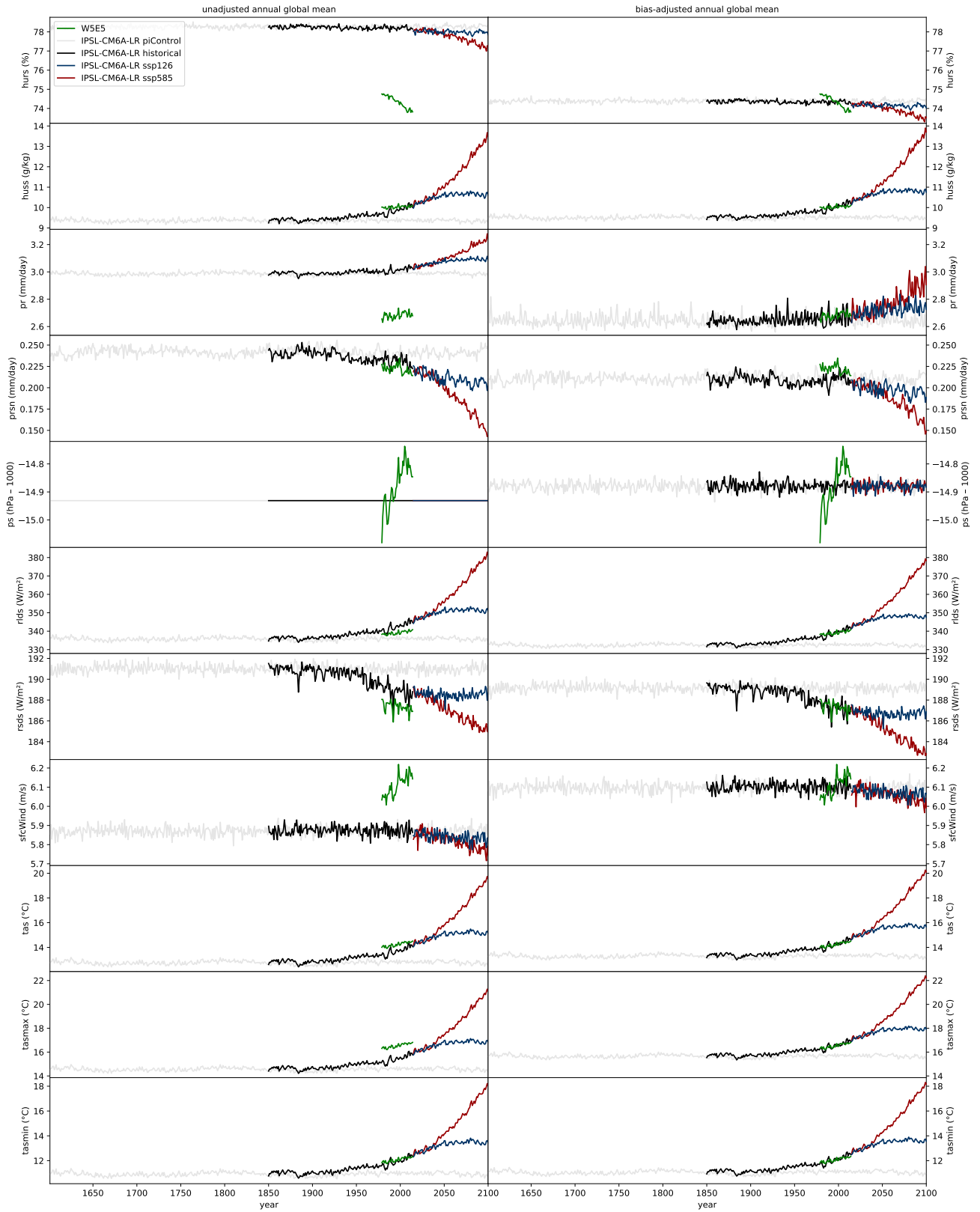


Figure 12: Same as Figure 9 but for IPSL-CM6A-LR.

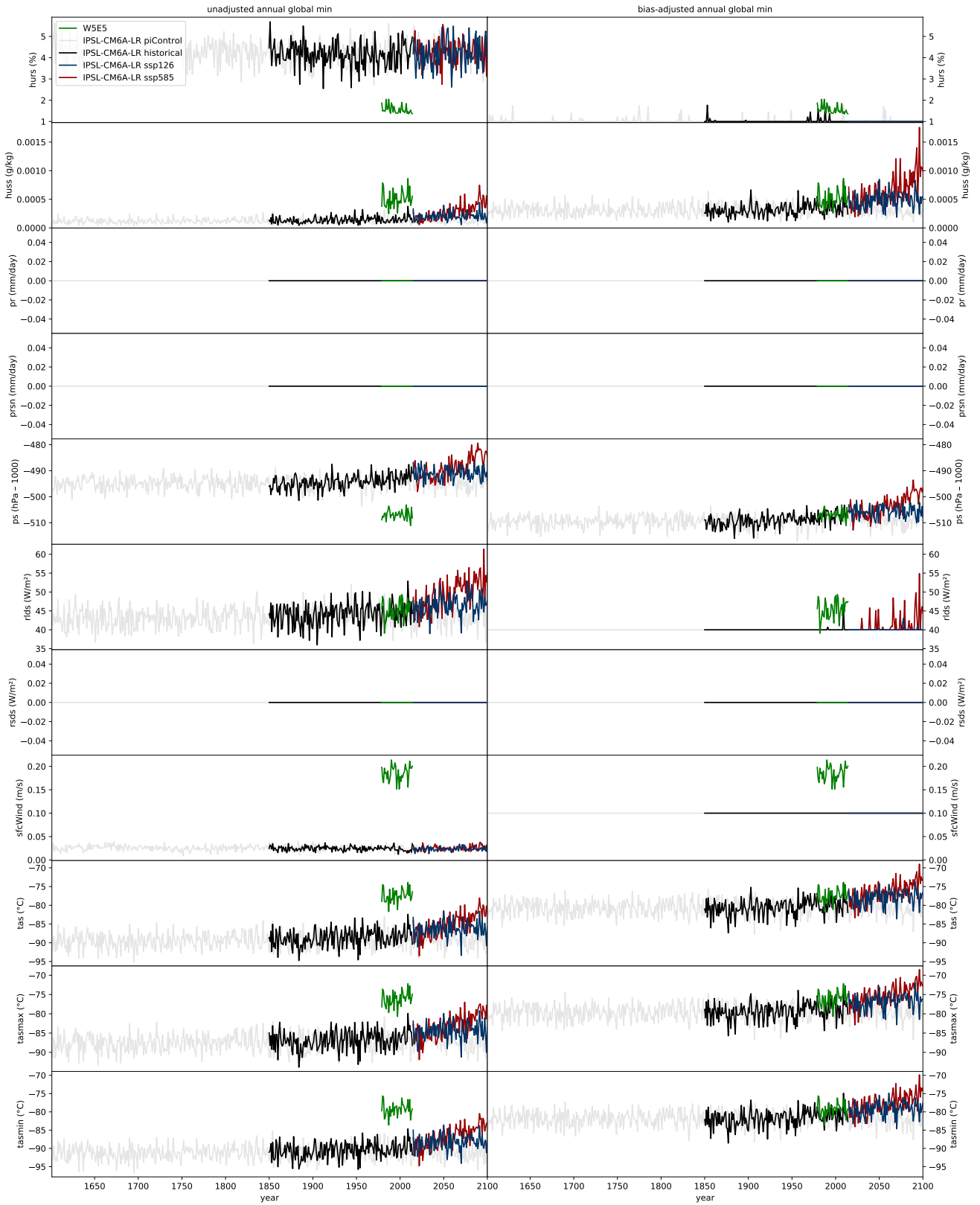


Figure 13: Same as Figure 10 but for IPSL-CM6A-LR.

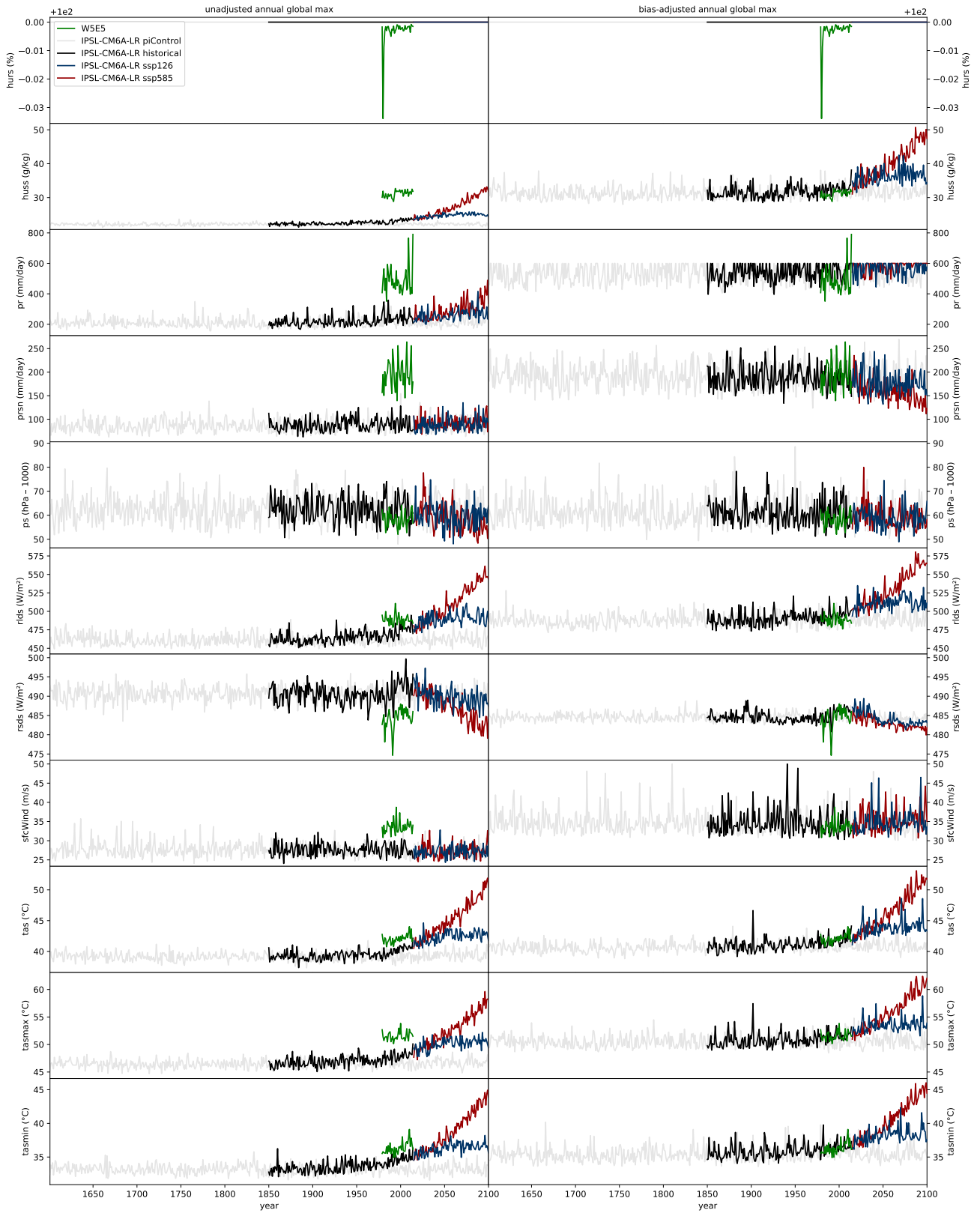


Figure 14: Same as Figure 11 but for IPSL-CM6A-LR.

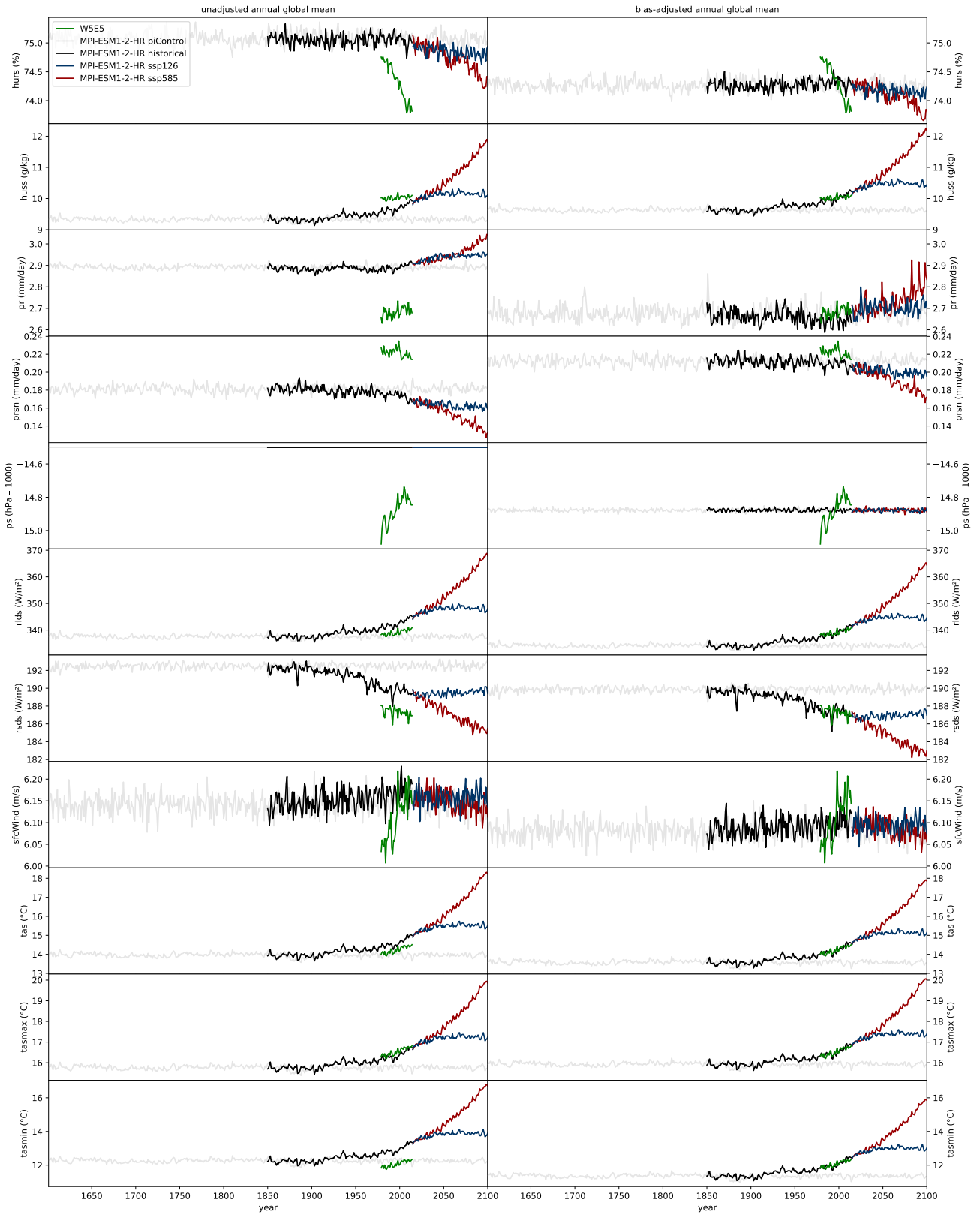


Figure 15: Same as Figure 9 but for MPI-ESM1-2-HR.

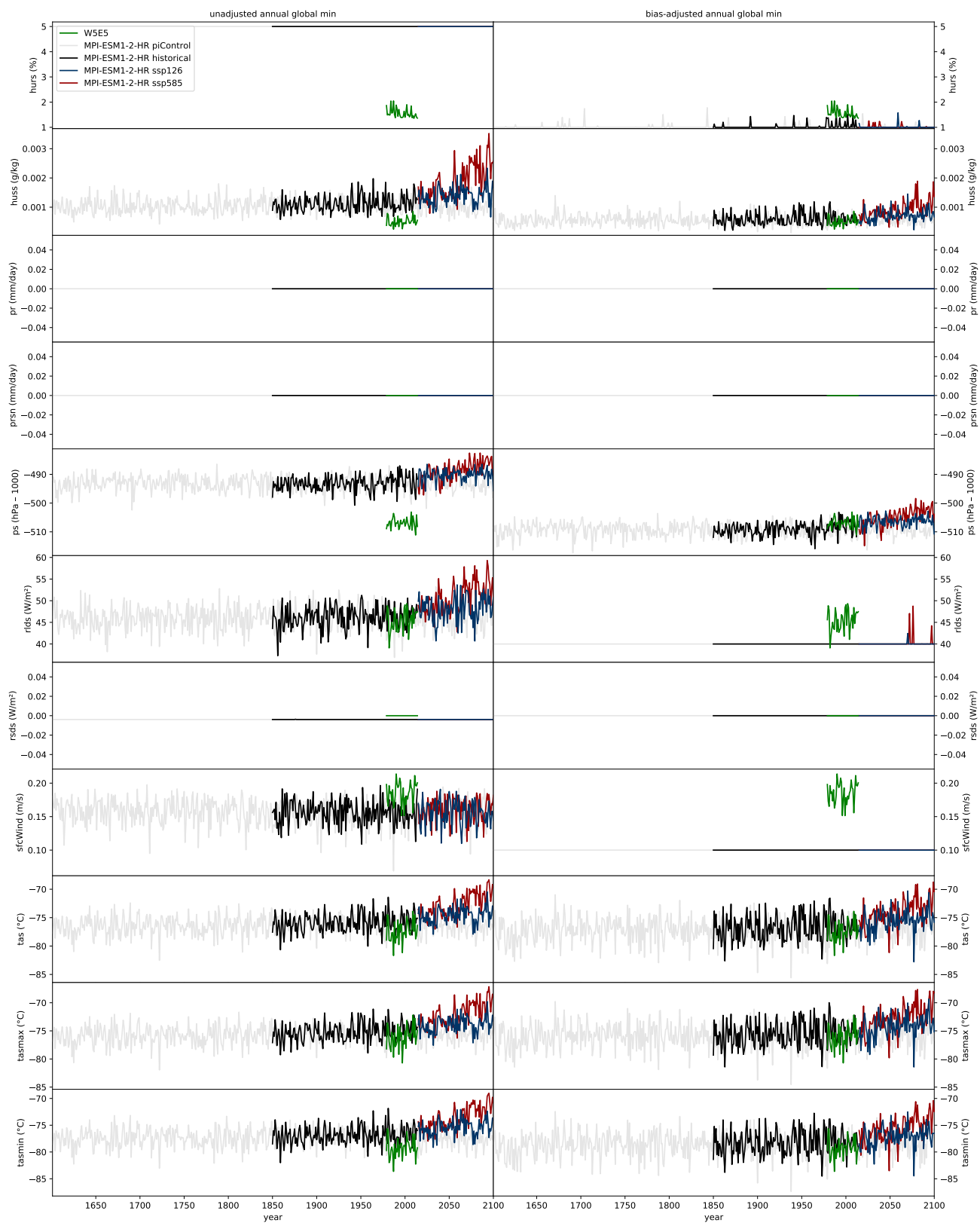


Figure 16: Same as Figure 10 but for MPI-ESM1-2-HR.

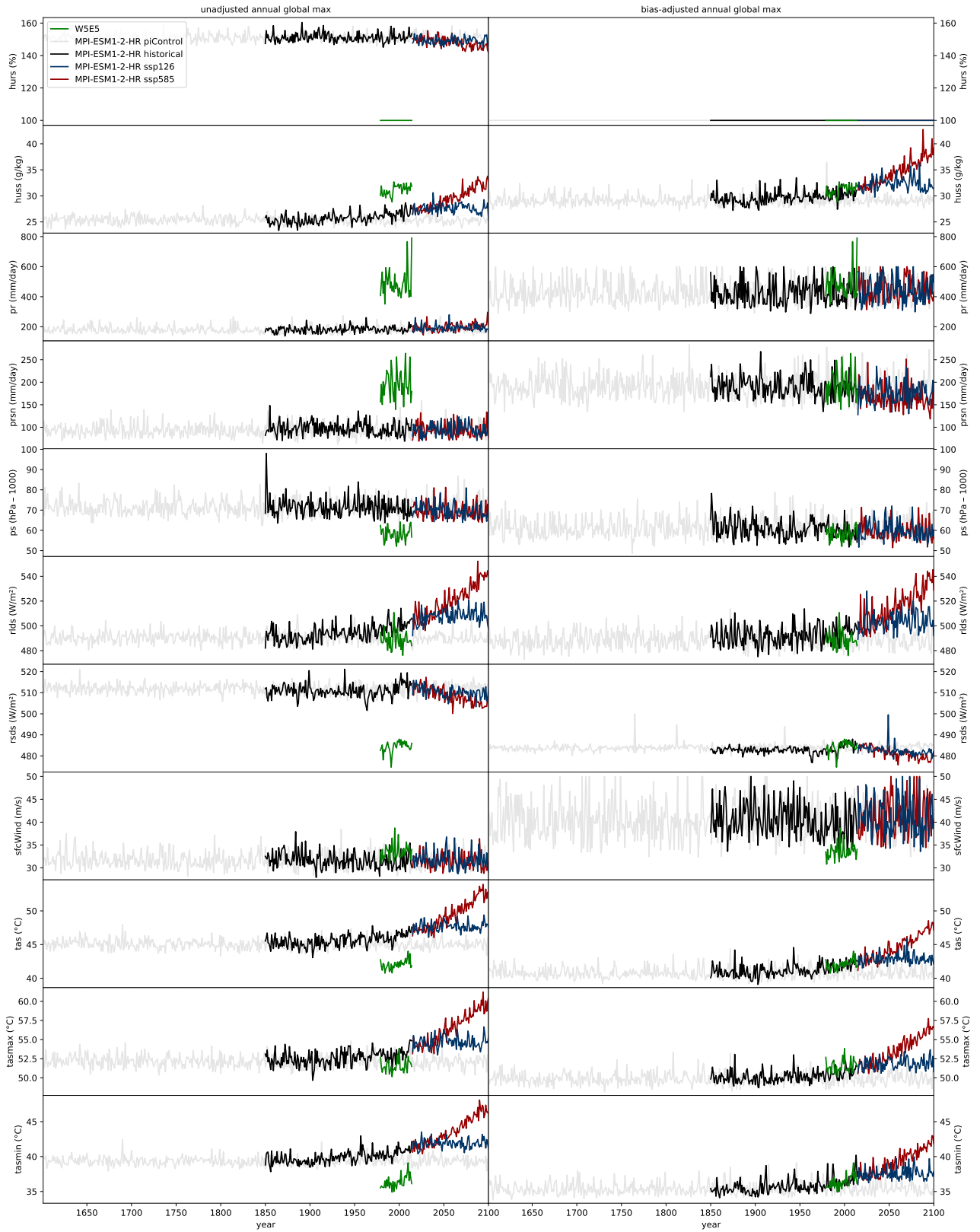


Figure 17: Same as Figure 11 but for MPI-ESM1-2-HR.

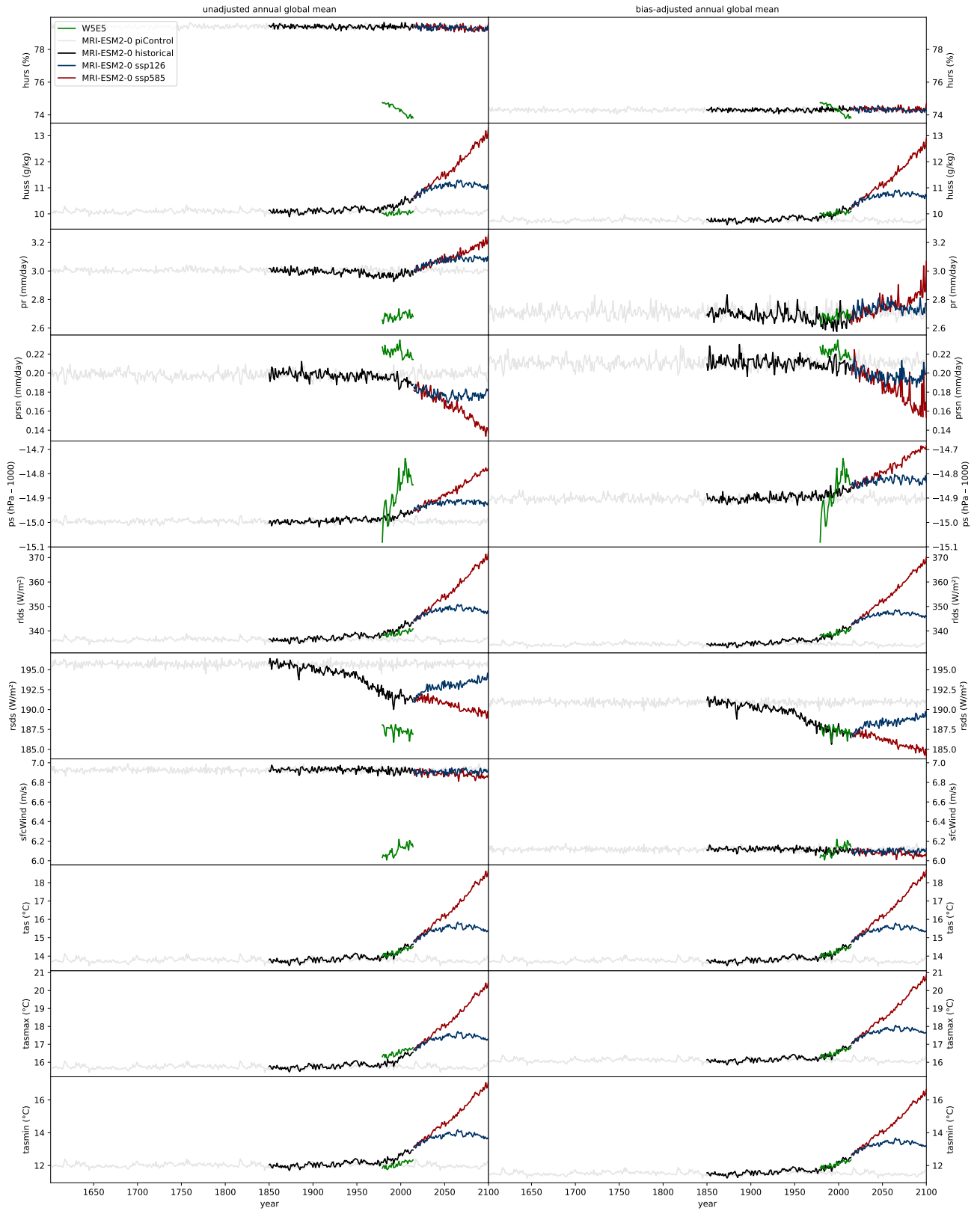


Figure 18: Same as Figure 9 but for MRI-ESM2-0.

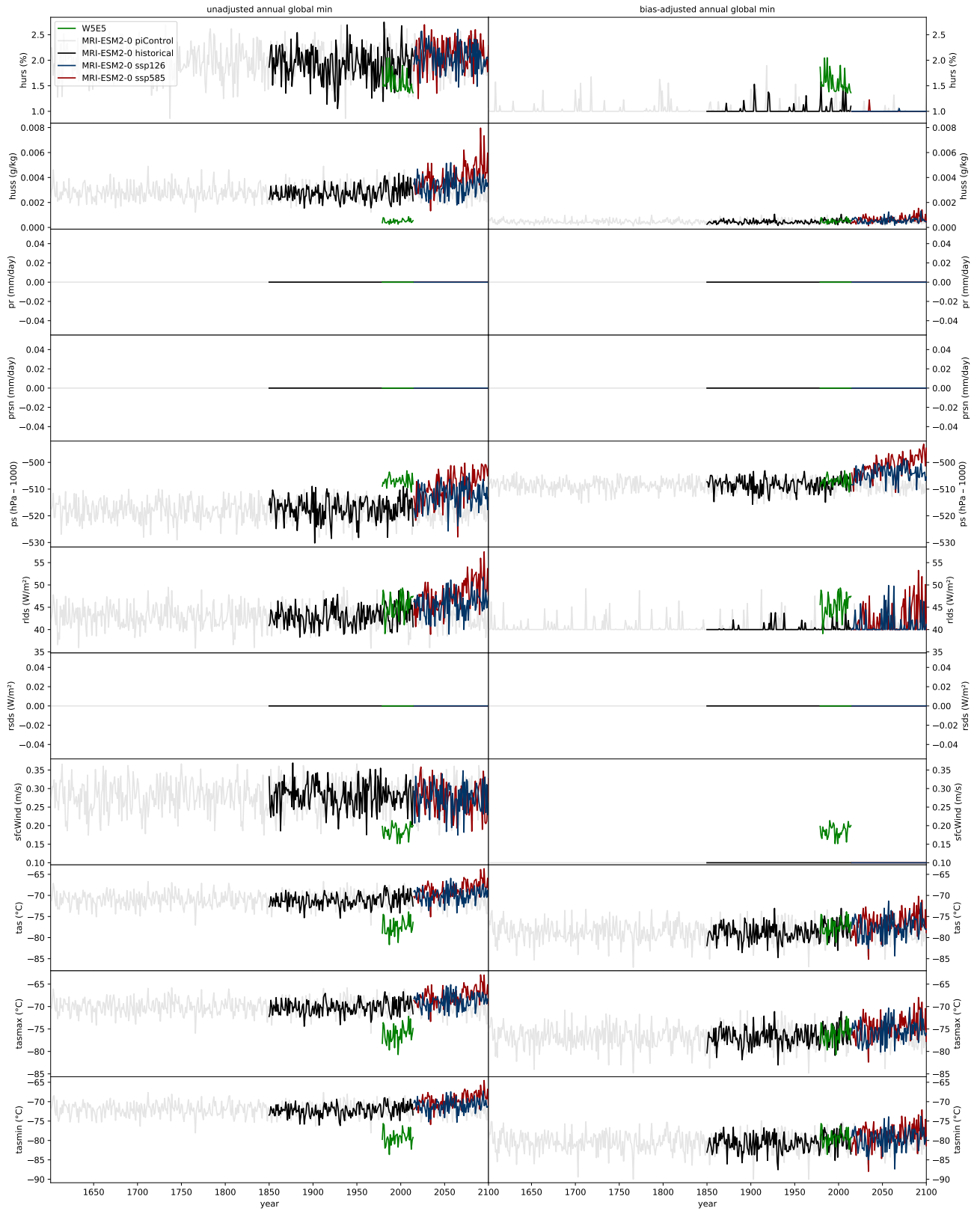


Figure 19: Same as Figure 10 but for MRI-ESM2-0.

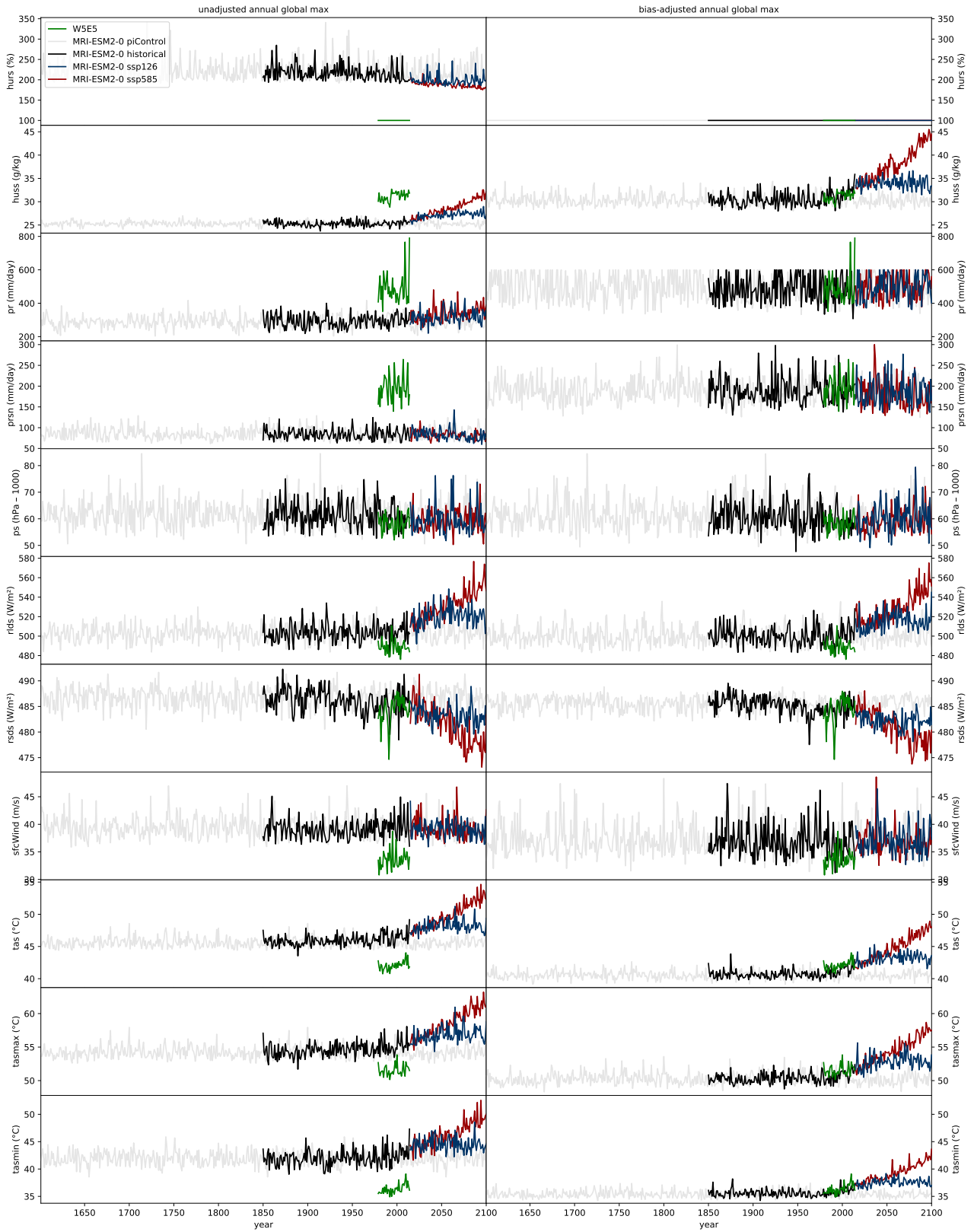


Figure 20: Same as Figure 11 but for MRI-ESM2-0.

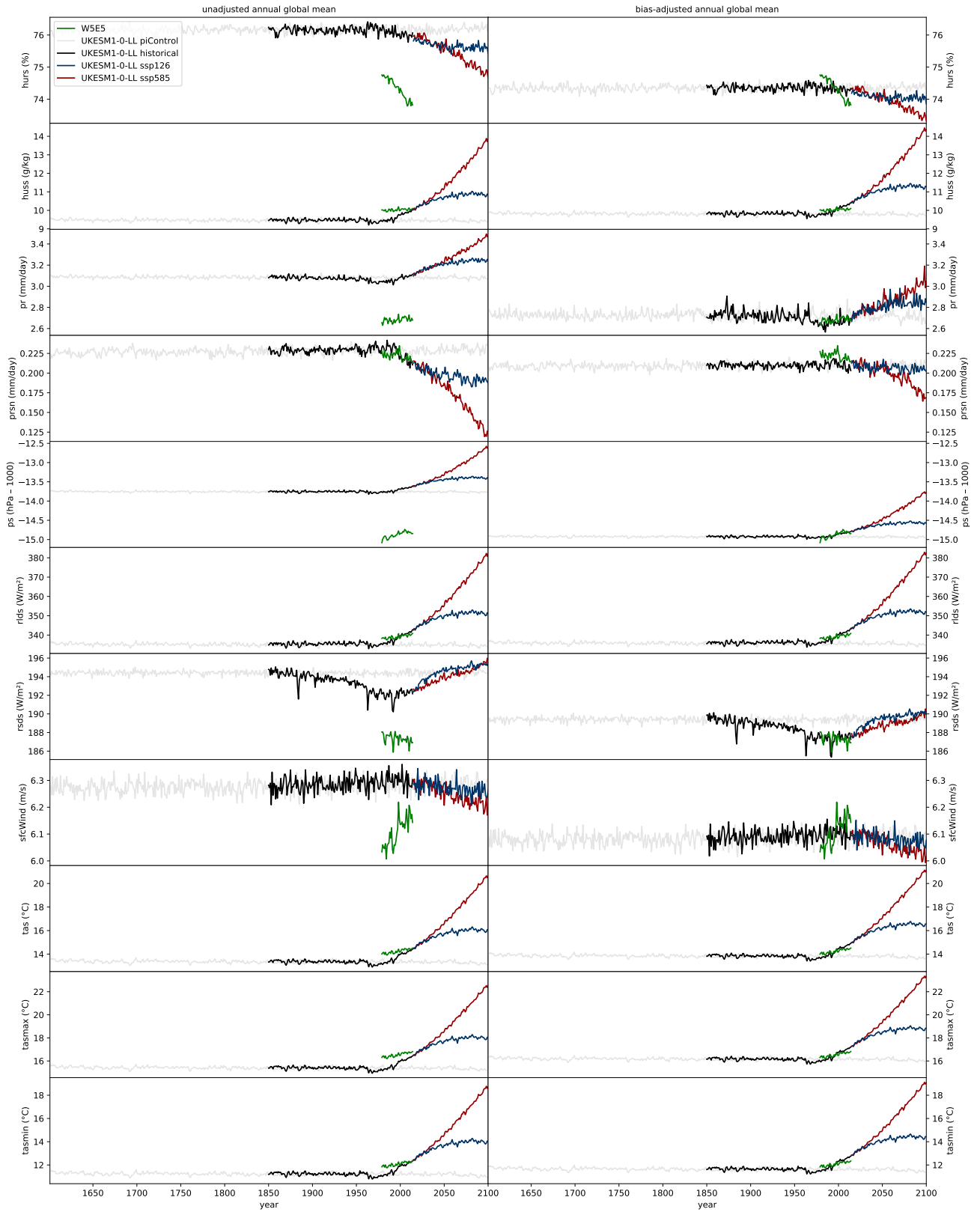


Figure 21: Same as Figure 9 but for UKESM1-0-LL.

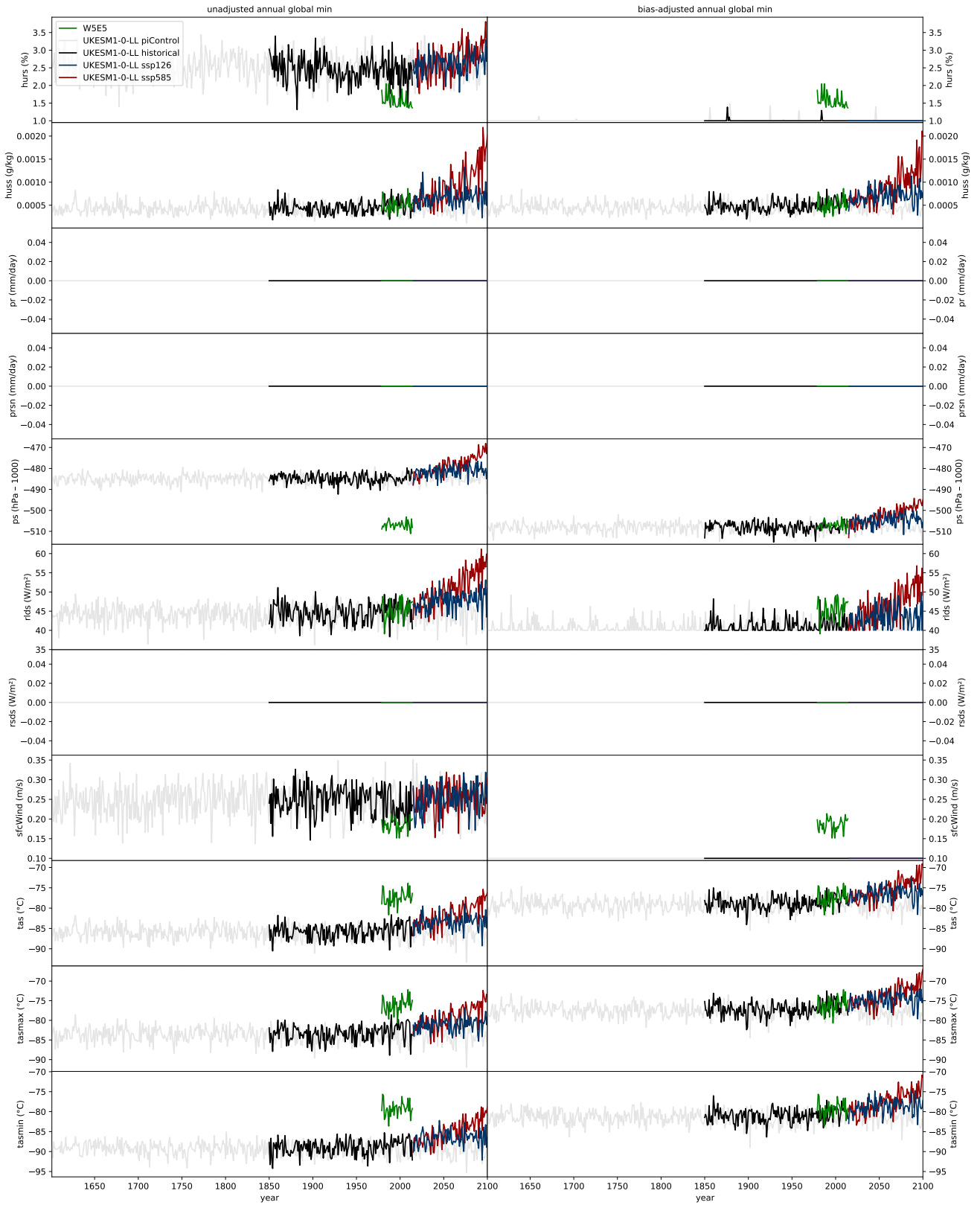


Figure 22: Same as Figure 10 but for UKESM1-0-LL.

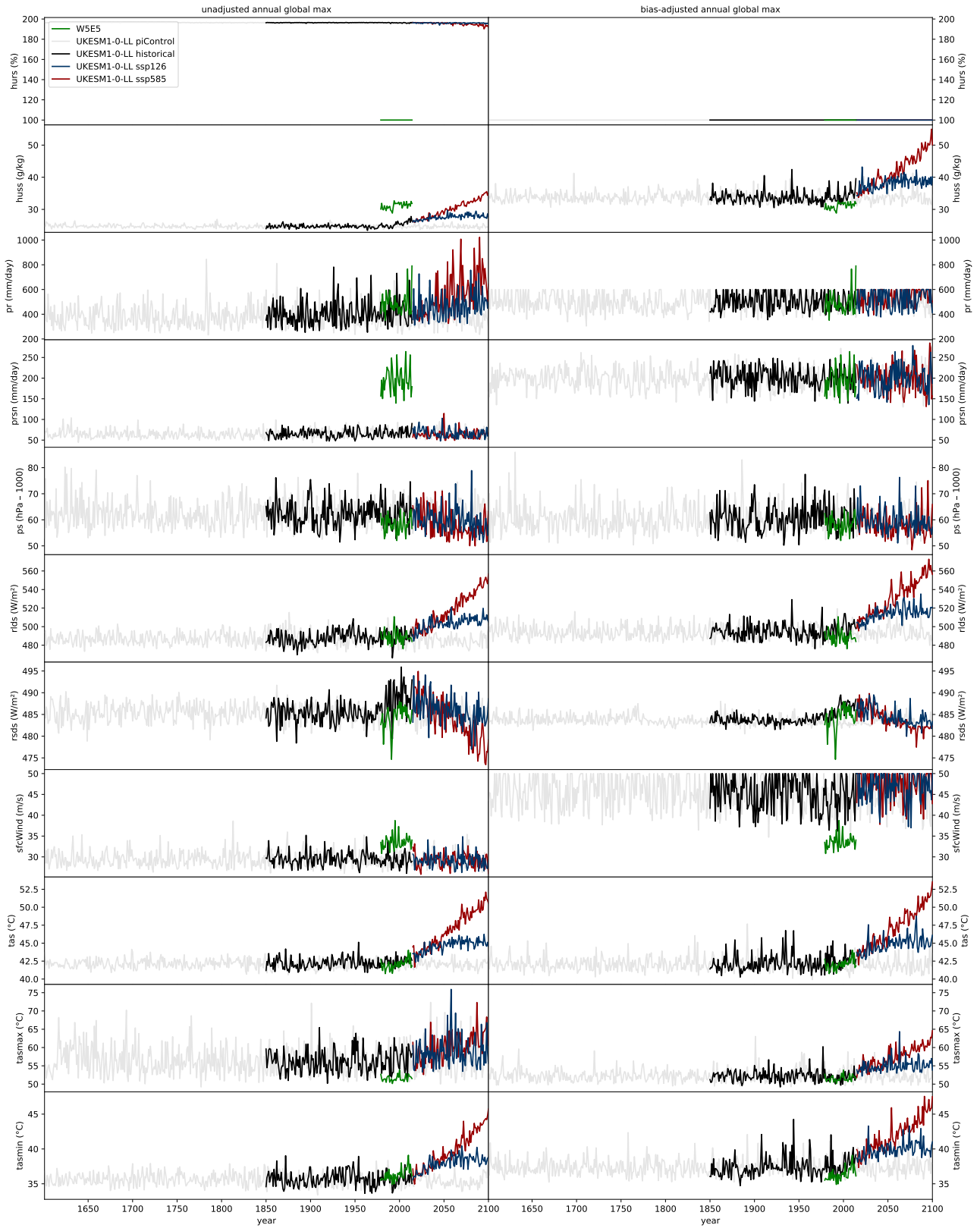


Figure 23: Same as Figure 11 but for UKESM1-0-LL.

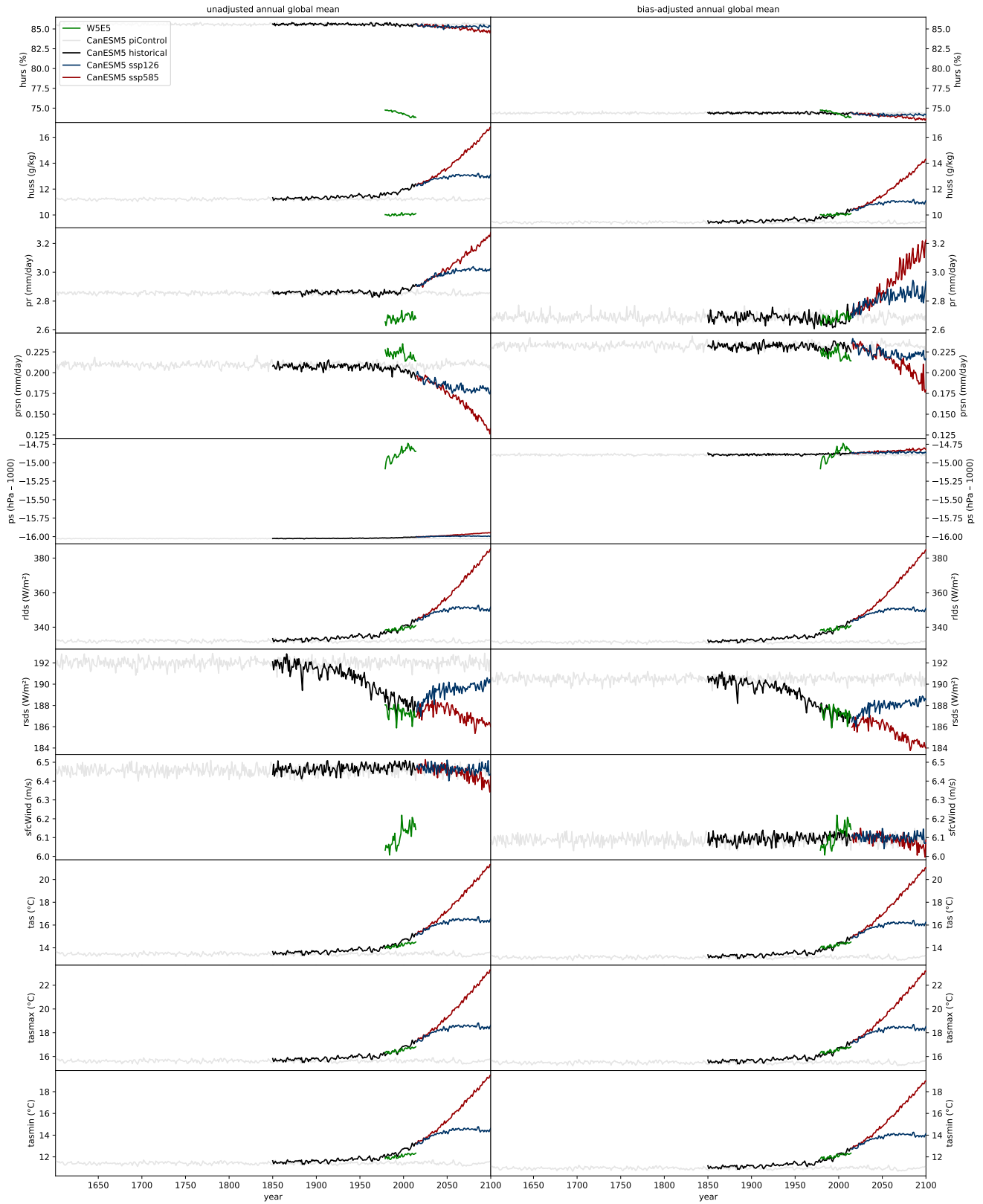


Figure 24: Same as Figure 9 but for CanESM5.

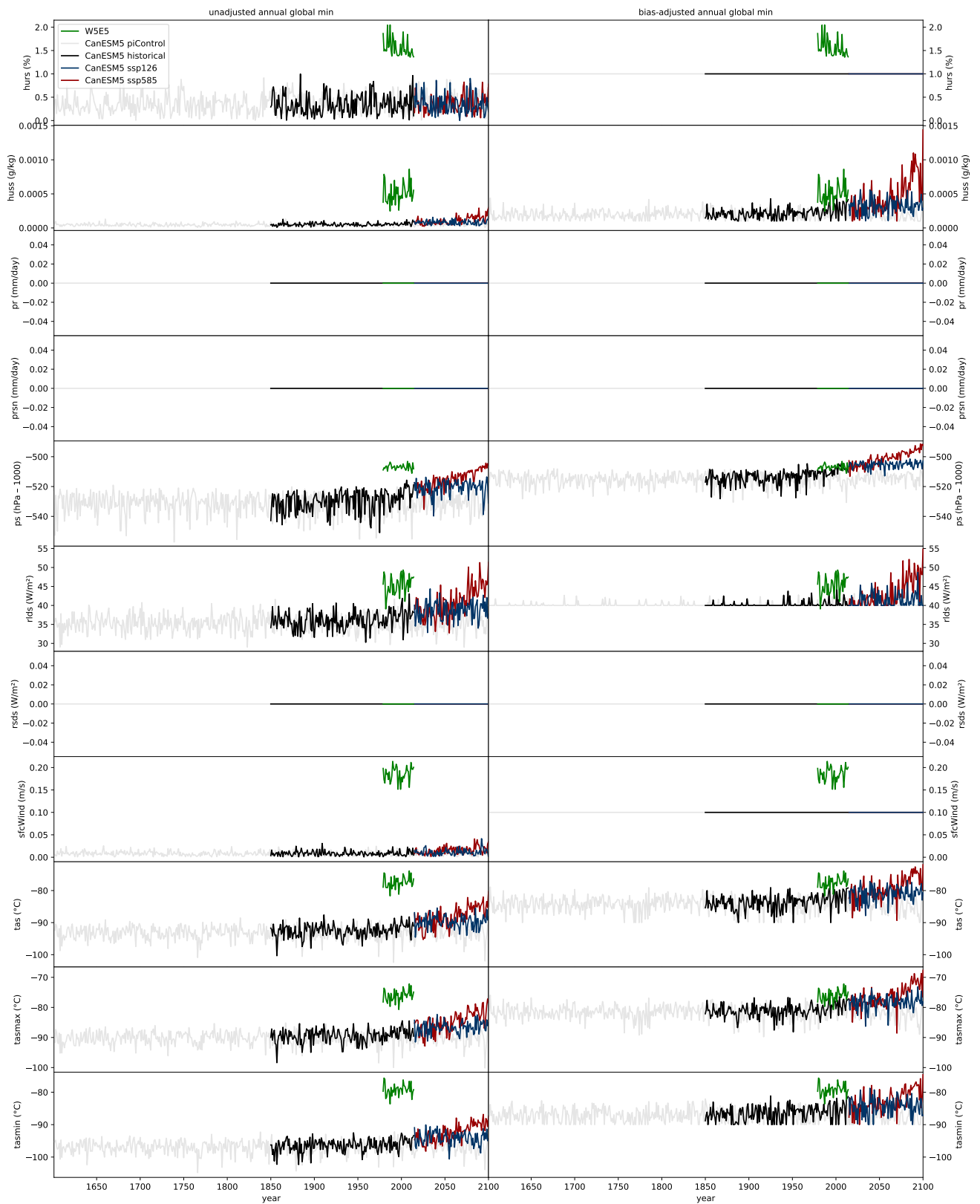


Figure 25: Same as Figure 10 but for CanESM5.

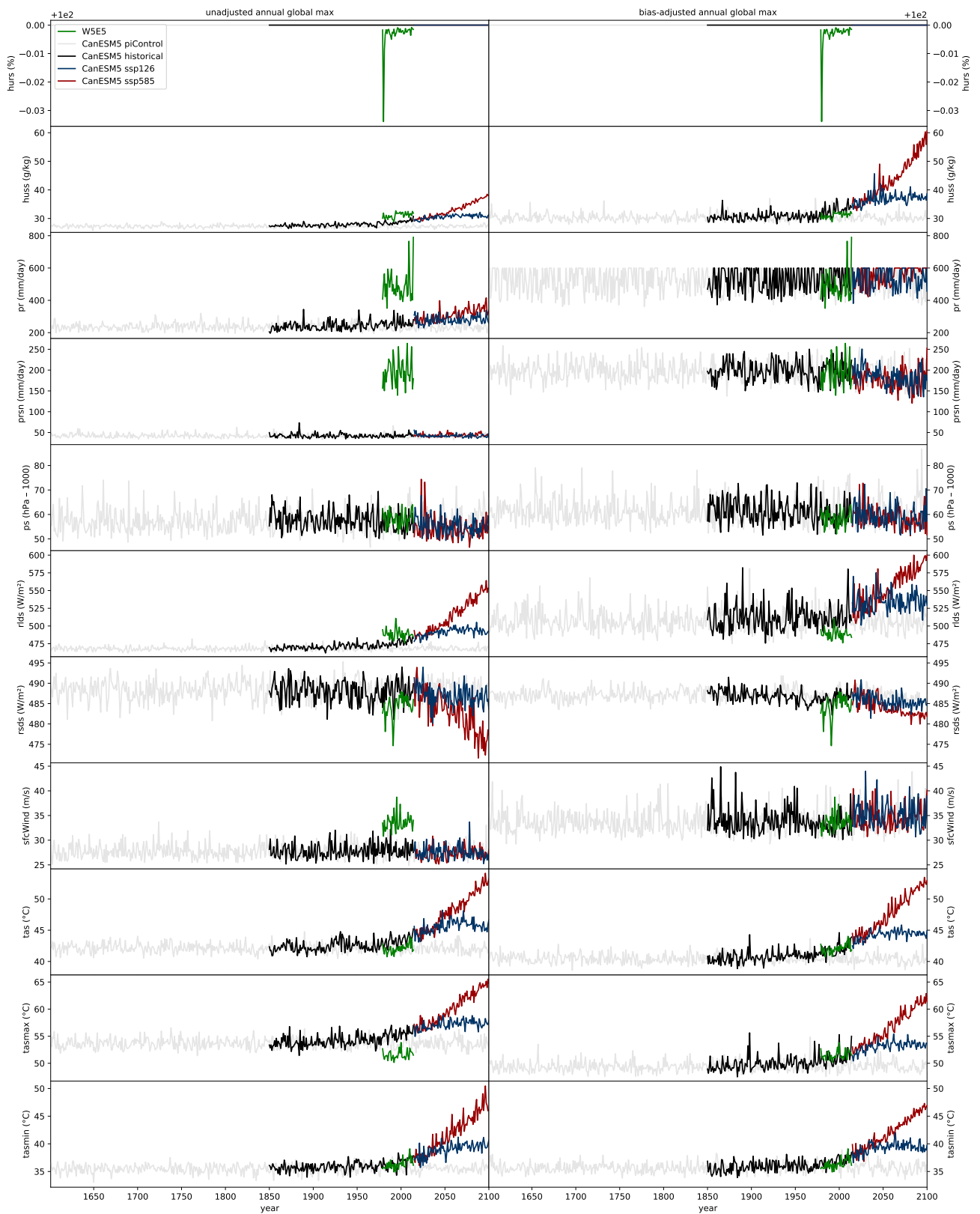


Figure 26: Same as Figure 11 but for CanESM5.

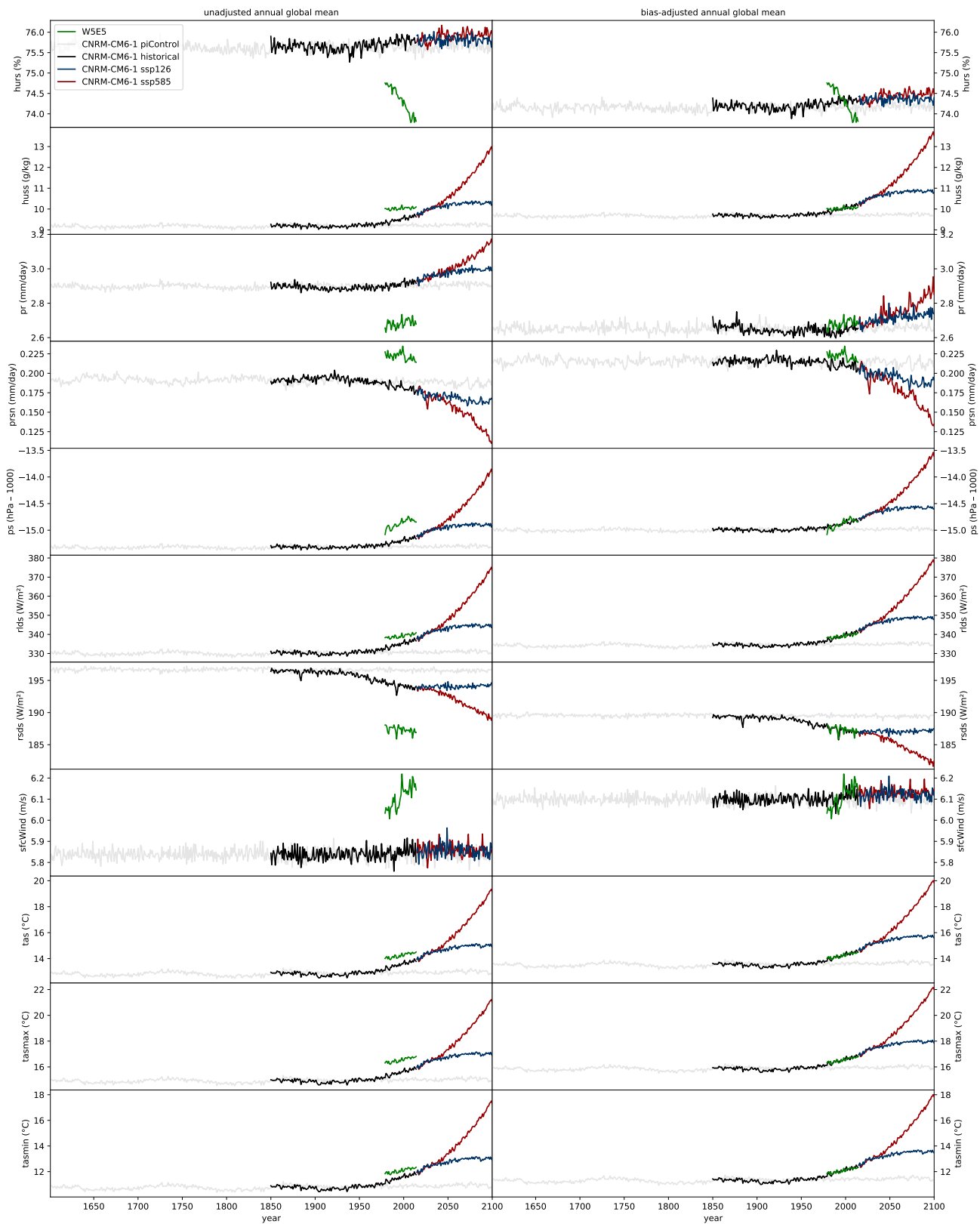


Figure 27: Same as Figure 9 but for CNRM-CM6-1.

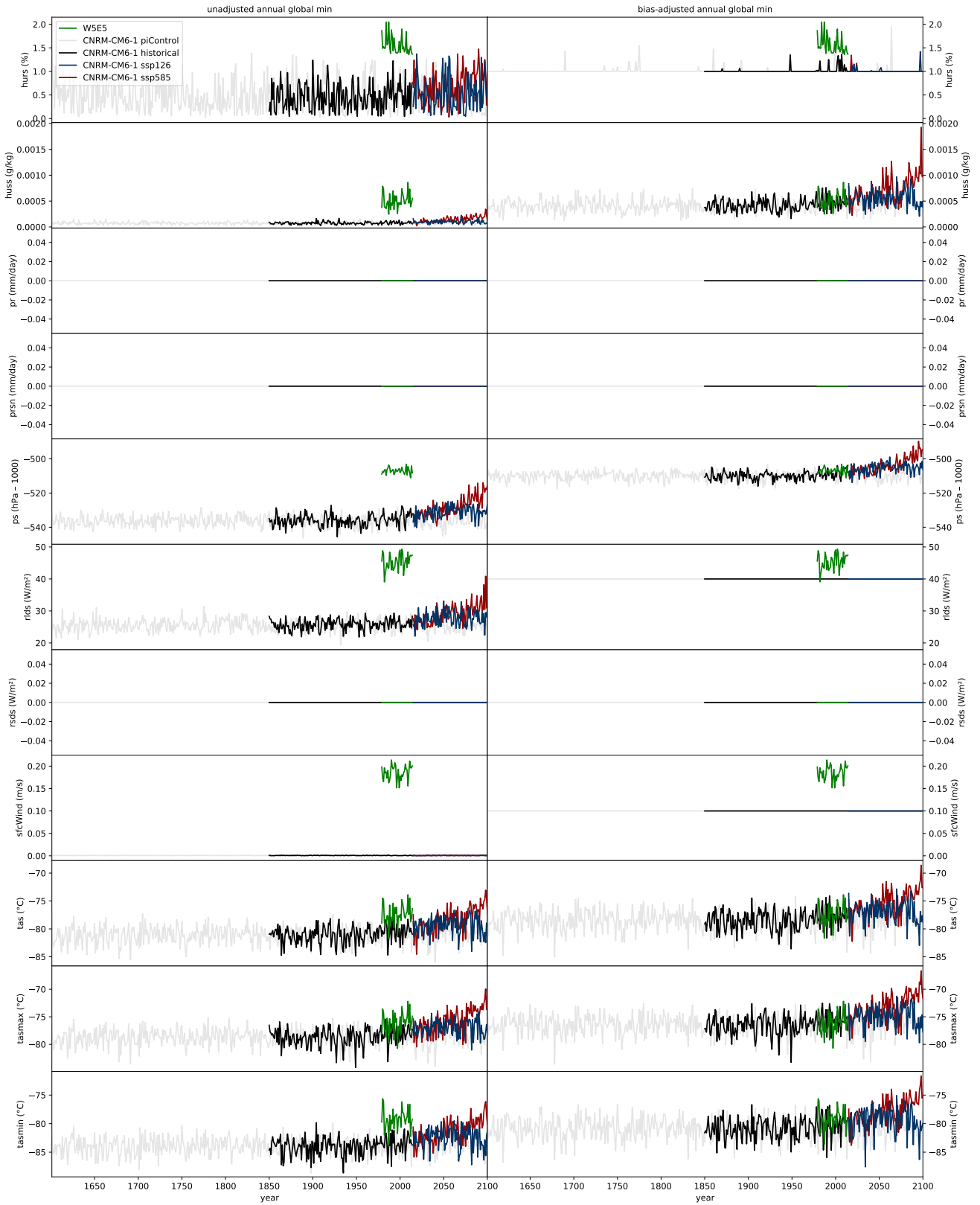


Figure 28: Same as Figure 10 but for CNRM-CM6-1.

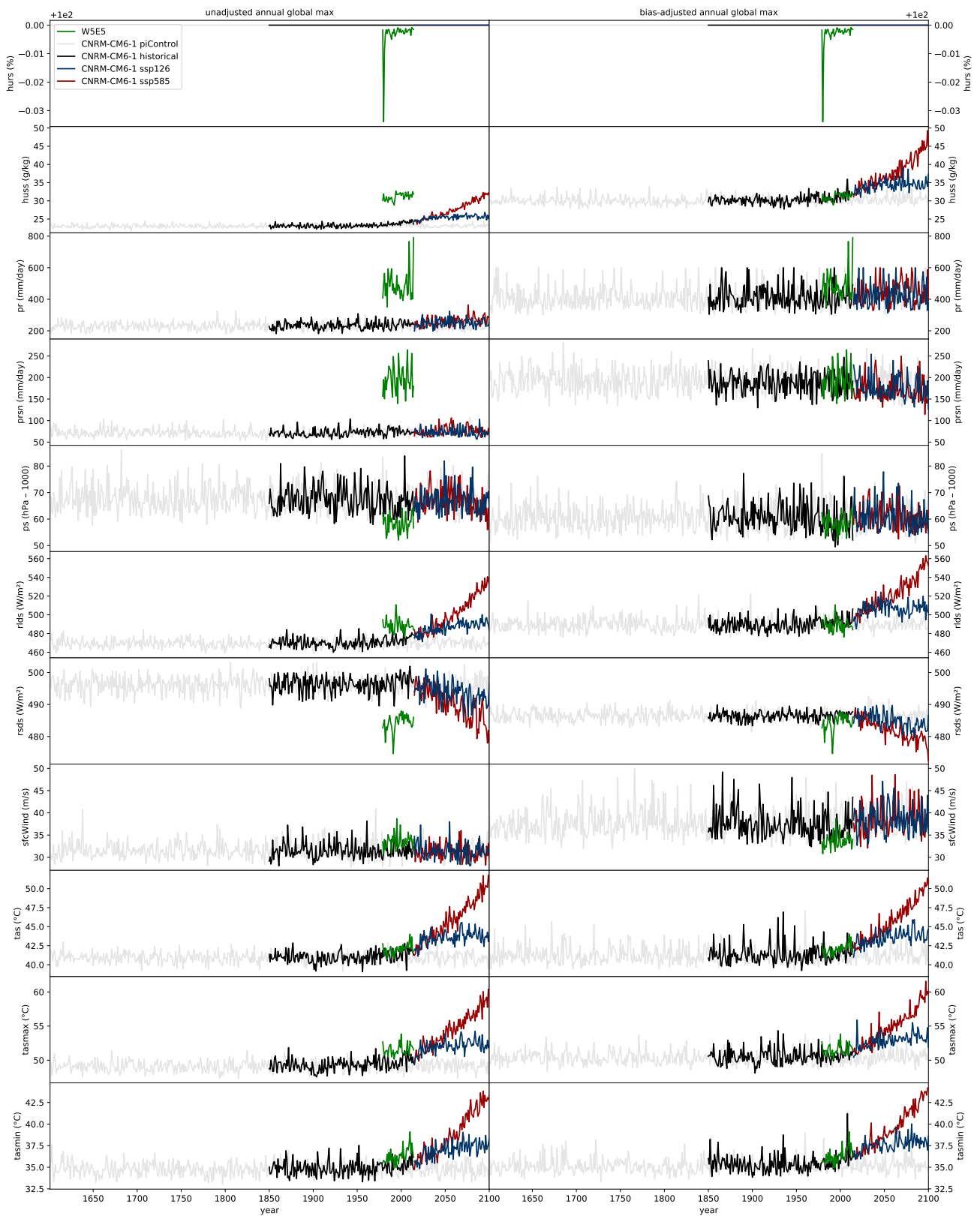


Figure 29: Same as Figure 11 but for CNRM-CM6-1.

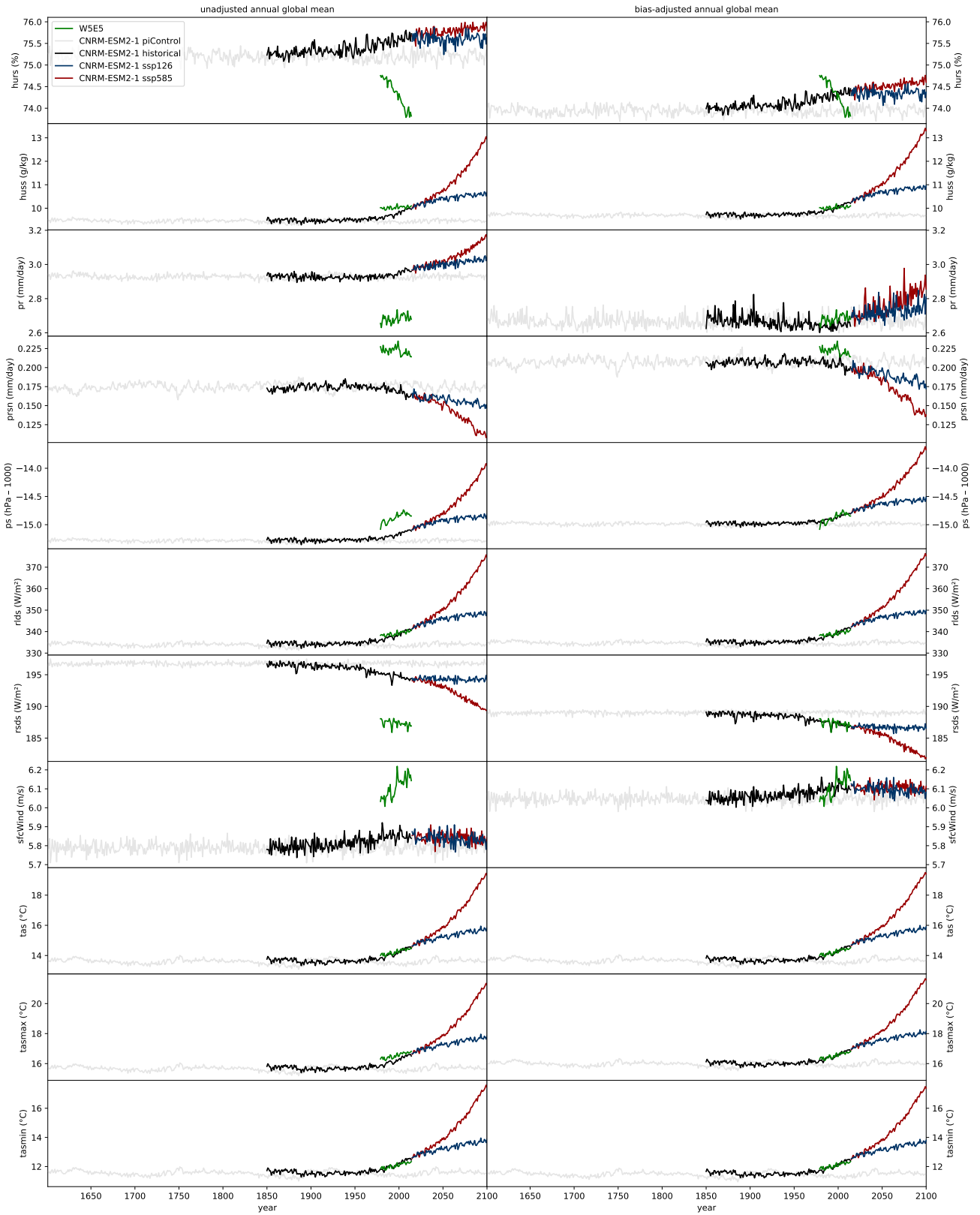


Figure 30: Same as Figure 9 but for CNRM-ESM2-1.

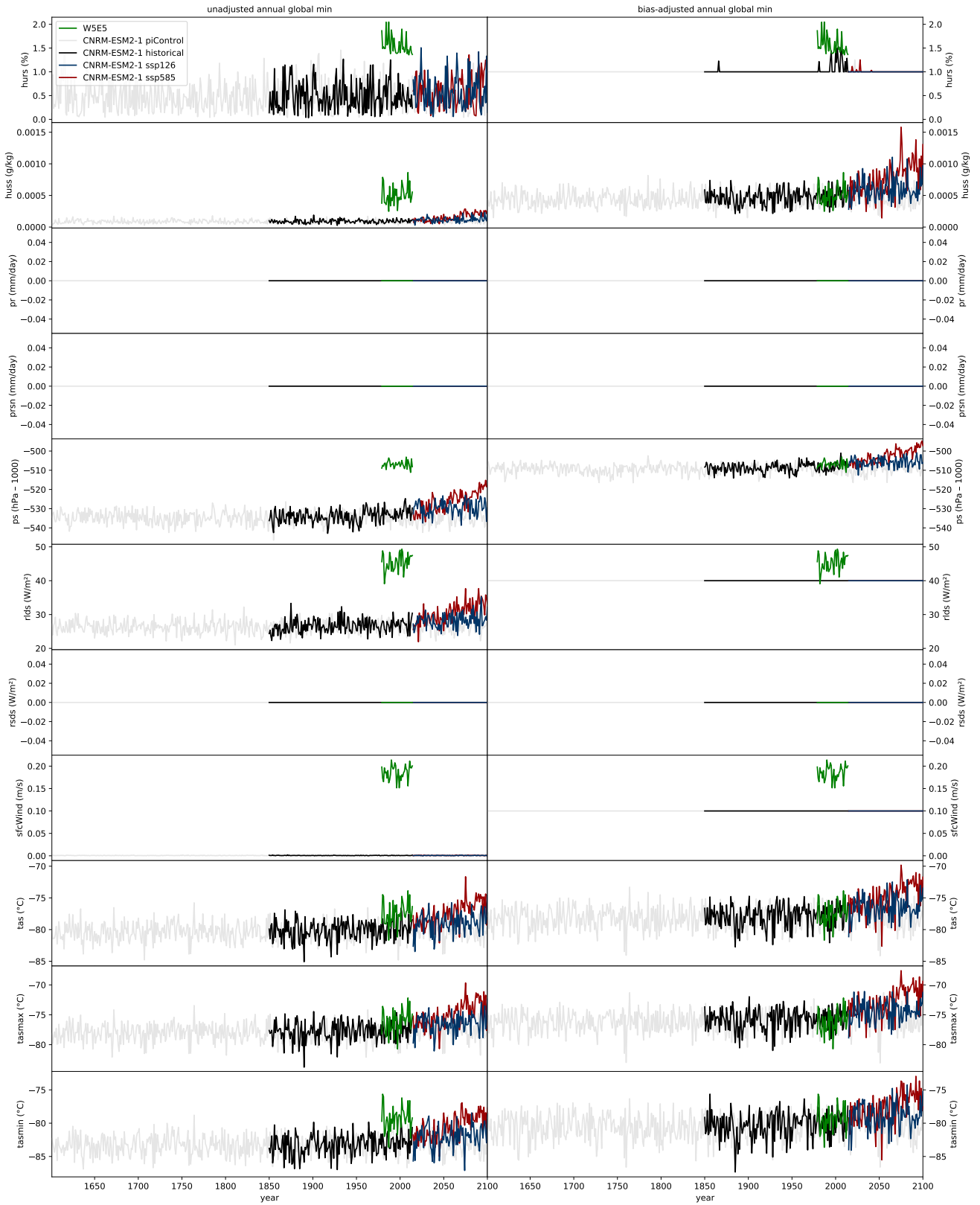


Figure 31: Same as Figure 10 but for CNRM-ESM2-1.

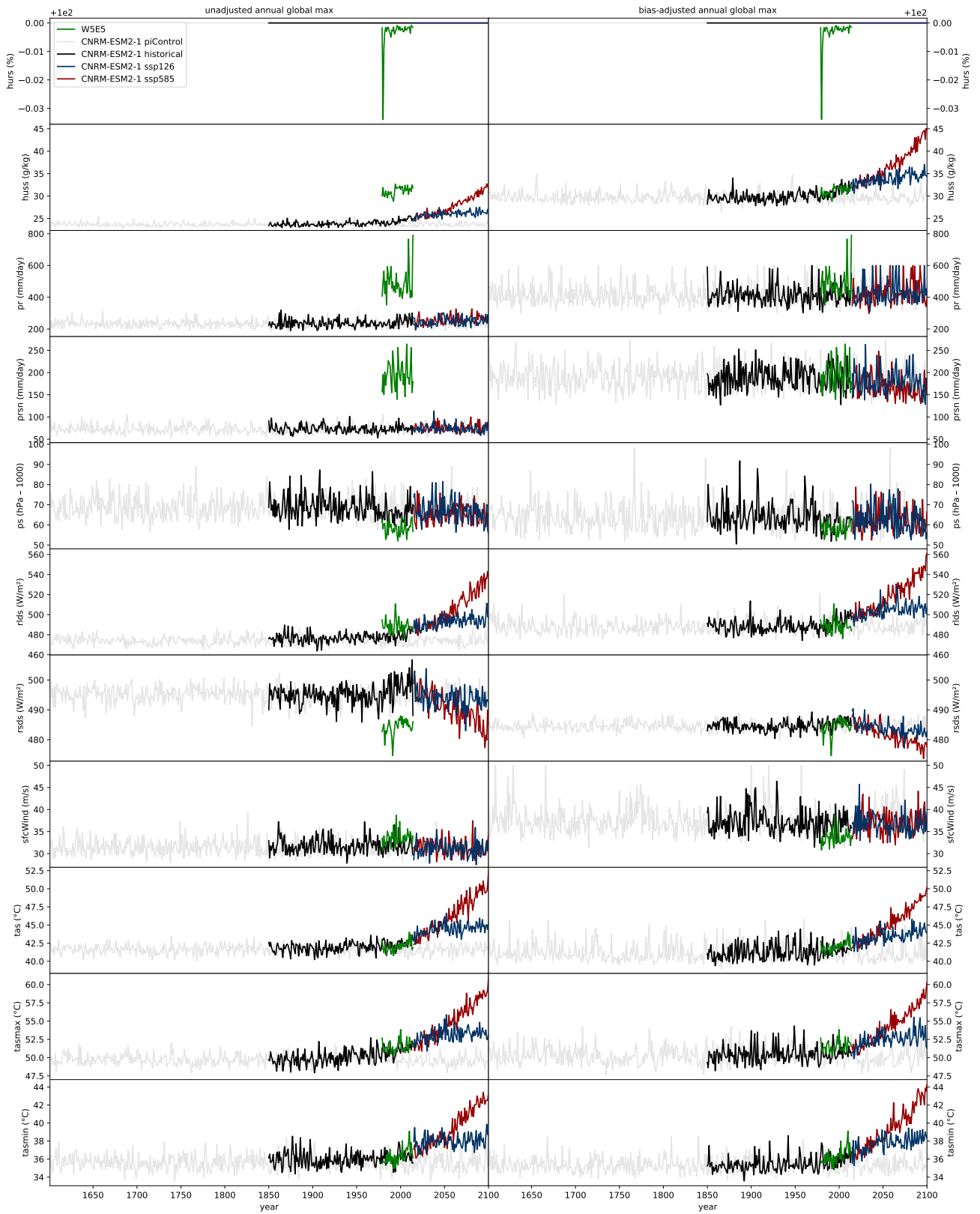


Figure 32: Same as Figure 11 but for CNRM-ESM2-1.

Figure 33: Same as Figure 9 but for EC-Earth3.

Figure 34: Same as Figure 10 but for EC-Earth3.

Figure 35: Same as Figure 11 but for EC-Earth3.

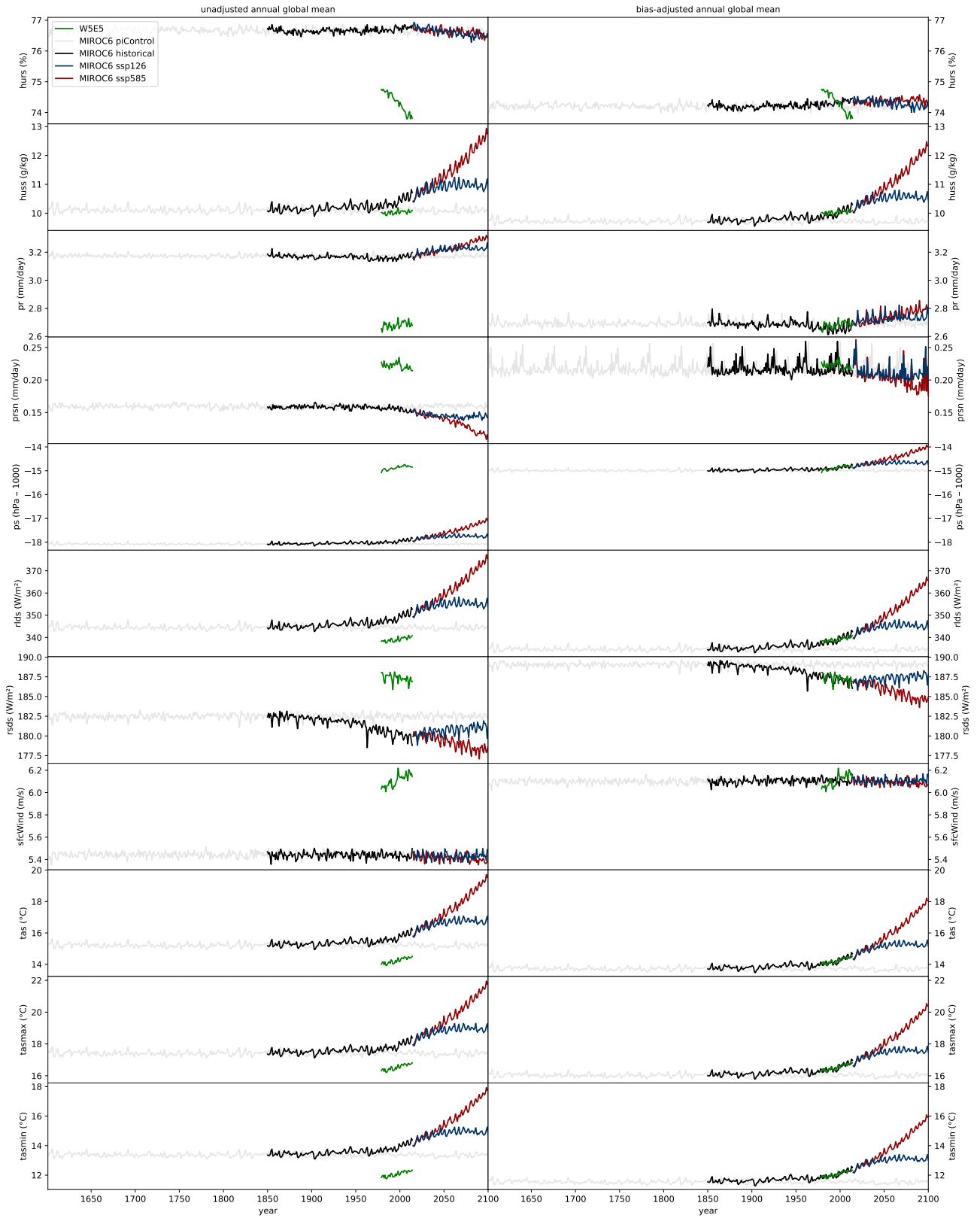


Figure 36: Same as Figure 9 but for MIROC6.

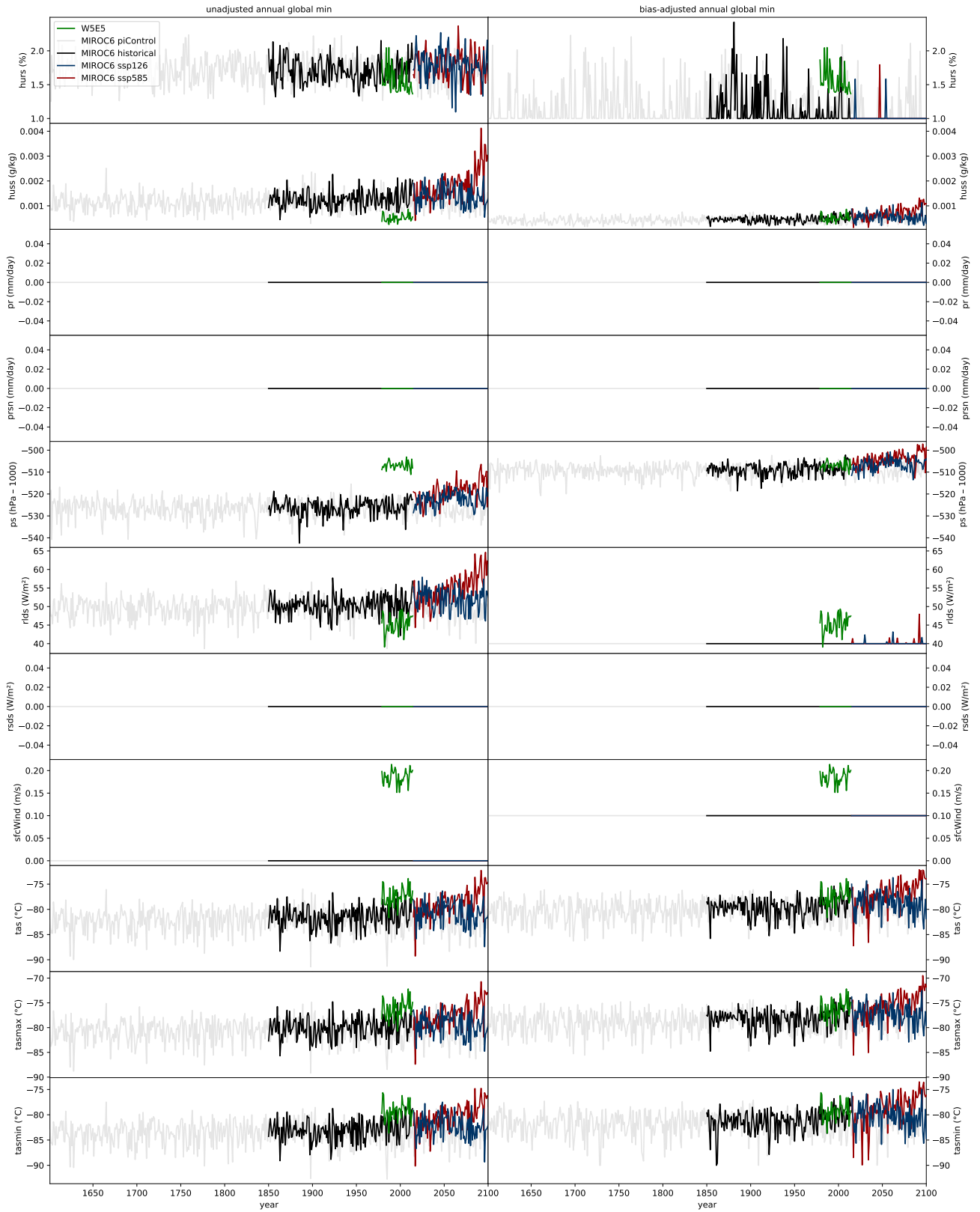


Figure 37: Same as Figure 10 but for MIROC6.

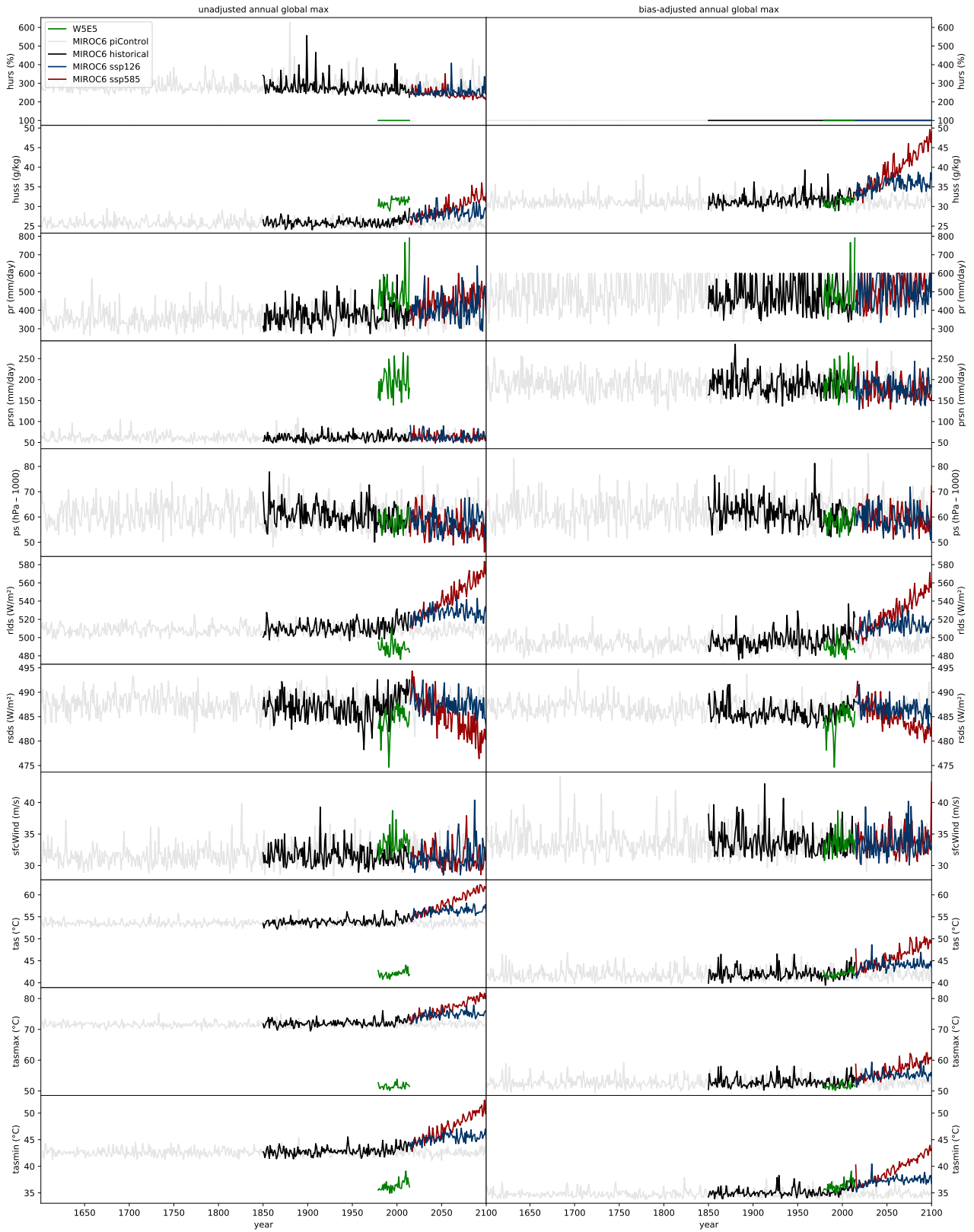


Figure 38: Same as Figure 11 but for MIROC6.

References

- Adler, R. F., Huffman, G. J., Chang, A., Ferraro, R., Xie, P.-P., Janowiak, J., Rudolf, B., Schneider, U., Curtis, S., Bolvin, D., Gruber, A., Susskind, J., Arkin, P., and Nelkin, E.: The Version-2 Global Precipitation Climatology Project (GPCP) Monthly Precipitation Analysis (1979–Present), *Journal of Hydrometeorology*, 4, 1147–1167, [https://doi.org/10.1175/1525-7541\(2003\)004<1147:TVGPCP>2.0.CO;2](https://doi.org/10.1175/1525-7541(2003)004<1147:TVGPCP>2.0.CO;2), 2003.
- Cannon, A. J.: Multivariate quantile mapping bias correction: an N-dimensional probability density function transform for climate model simulations of multiple variables, *Climate Dynamics*, pp. 1–19, <https://doi.org/10.1007/s00382-017-3580-6>, 2017.
- Cucchi, M., Weedon, G. P., Amici, A., Bellouin, N., Lange, S., Müller Schmied, H., Hersbach, H., and Buontempo, C.: WFDE5: bias-adjusted ERA5 reanalysis data for impact studies, *Earth System Science Data*, 12, 2097–2120, <https://doi.org/10.5194/essd-12-2097-2020>, 2020.
- Eyring, V., Bony, S., Meehl, G. A., Senior, C. A., Stevens, B., Stouffer, R. J., and Taylor, K. E.: Overview of the Coupled Model Intercomparison Project Phase 6 (CMIP6) experimental design and organization, *Geoscientific Model Development*, 9, 1937–1958, <https://doi.org/10.5194/gmd-9-1937-2016>, 2016.
- Gennaretti, F., Sangelantoni, L., and Grenier, P.: Toward daily climate scenarios for Canadian Arctic coastal zones with more realistic temperature-precipitation interdependence, *Journal of Geophysical Research: Atmospheres*, 120, 11,862–11,877, <https://doi.org/10.1002/2015JD023890>, 2015.
- Gleckler, P. J., Taylor, K. E., and Doutriaux, C.: Performance metrics for climate models, *Journal of Geophysical Research: Atmospheres*, 113, <https://doi.org/10.1029/2007JD008972>, 2008.
- Grenier, P.: Two Types of Physical Inconsistency to Avoid with Univariate Quantile Mapping: A Case Study over North America Concerning Relative Humidity and Its Parent Variables, *Journal of Applied Meteorology and Climatology*, 57, 347–364, <https://doi.org/10.1175/JAMC-D-17-0177.1>, 2018.
- Hersbach, H., Bell, B., Berrisford, P., Hirahara, S., Horányi, A., Muñoz-Sabater, J., Nicolas, J., Peubey, C., Radu, R., Schepers, D., Simmons, A., Soci, C., Abdalla, S., Abellan, X., Balsamo, G., Bechtold, P., Biavati, G., Bidlot, J., Bonavita, M., De Chiara, G., Dahlgren, P., Dee, D., Diamantakis, M., Dragani, R., Flemming, J., Forbes, R., Fuentes, M., Geer, A., Haimberger, L., Healy, S., Hogan, R. J., Hólm, E., Janisková, M., Keeley, S., Laloyaux, P., Lopez, P., Lupu, C., Radnoti, G., de Rosnay, P., Rozum, I., Vamborg, F., Villaume, S., and Thépaut, J.-N.: The ERA5 Global Reanalysis, *Quarterly Journal of the Royal Meteorological Society*, <https://doi.org/10.1002/qj.3803>, 2020.
- Jones, P. W.: First- and Second-Order Conservative Remapping Schemes for Grids in Spherical Coordinates, *Monthly Weather Review*, 127, 2204–2210, [https://doi.org/10.1175/1520-0493\(1999\)127<2204:FASOCR>2.0.CO;2](https://doi.org/10.1175/1520-0493(1999)127<2204:FASOCR>2.0.CO;2), 1999.
- Lange, S.: Trend-preserving bias adjustment and statistical downscaling with ISIMIP3BASD (v1.0), *Geoscientific Model Development*, 12, 3055–3070, <https://doi.org/10.5194/gmd-12-3055-2019>, 2019.
- Lange, S.: ISIMIP3BASD v2.5.0, <https://doi.org/10.5281/zenodo.4686991>, 2021.
- Lange, S., Menz, C., Gleixner, S., Cucchi, M., Weedon, G. P., Amici, A., Bellouin, N., Schmied, H. M., Hersbach, H., Buontempo, C., and Cagnazzo, C.: WFDE5 over land merged with ERA5 over the ocean (W5E5 v2.0), <https://doi.org/10.48364/ISIMIP.342217>, 2021.
- Ruosteenoja, K., Jylhä, K., Räisänen, J., and Mäkelä, A.: Surface air relative humidities spuriously exceeding 100 % in CMIP5 model output and their impact on future projections, *Journal of Geophysical Research: Atmospheres*, 122, 9557–9568, <https://doi.org/10.1002/2017JD026909>, 2017.

- Ruosteenoja, K., Jylhä, K., Räisänen, J., and Mäkelä, A.: Reply to Comment by Genthon et al. on "Surface Air Relative Humidities Spuriously Exceeding 100 % in CMIP5 Model Output and Their Impact on Future Projections", *Journal of Geophysical Research: Atmospheres*, 123, 8728–8734, <https://doi.org/10.1029/2018JD028680>, 2018.
- Thiemeßl, M. J., Gobiet, A., and Heinrich, G.: Empirical-statistical downscaling and error correction of regional climate models and its impact on the climate change signal, *Climatic Change*, 112, 449–468, <https://doi.org/10.1007/s10584-011-0224-4>, 2012.
- Thrasher, B., Maurer, E. P., McKellar, C., and Duffy, P. B.: Technical Note: Bias correcting climate model simulated daily temperature extremes with quantile mapping, *Hydrology and Earth System Sciences*, 16, 3309–3314, <https://doi.org/10.5194/hess-16-3309-2012>, 2012.
- Weedon, G. P., Balsamo, G., Bellouin, N., Gomes, S., Best, M. J., and Viterbo, P.: The WFDEI meteorological forcing data set: WATCH Forcing Data methodology applied to ERA-Interim reanalysis data, *Water Resources Research*, 50, 7505–7514, <https://doi.org/10.1002/2014WR015638>, 2014.